Printing Proteins and Cell-Surface Interaction

Chapter 3

Chapter 4

SOFT LITHOGRAPHY

Annu. Rev. Mater. Sci. 1998. 28:153–84

Younan Xia and George M. Whitesides
Department of Chemistry and Chemical Biology, Harvard University, Cambridge, Massachusetts 02138; e-mail: gwhitesides@gmwgroup.harvard.edu

Table 1 Comparison between photolithography and soft lithography

	Photolithography	Soft lithography
Definition of patterns	Rigid photomask (patterned Cr supported on a quartz plate)	Elastomeric stamp or mold (a PDMS block patterned with relief features)
Materials that can be patterned directly	Photoresists (polymers with photo-sensitive additives)	Photoresists[a,e]
	SAMs on Au and SiO_2	SAMs on Au, Ag, Cu, GaAs, Al, Pd, and SiO_2[a] Unsensitized polymers[b–e] (epoxy, PU, PMMA, ABS, CA, PS, PE, PVC) Precursor polymers[c,d] (to carbons and ceramics) Polymer beads[d] Conducting polymers[d] Colloidal materials[a,d] Sol-gel materials[c,d] Organic and inorganic salts[d] Biological macromolecules[d]
Surfaces and structures that can be patterned	Planar surfaces 2-D structures	Both planar and nonplanar Both 2-D and 3-D structures
Current limits to resolution	~250 nm (projection) ~100 nm (laboratory)	~30 nm[a,b], ~60 nm[e], ~1 μm[d,e] (laboratory)
Minimum feature size	~100 nm (?)	10 (?) - 100 nm

[a–e]Made by (a) μCP, (b) REM, (c) μTM, (d) MIMIC, (e) SAMIM. PU:polyurethane; PMMA: poly(methyl methacrylate); ABS: poly(acrylonitrile-butadiene-styrene); CA: cellulose acetate; PS: polystyrene; PE: polyethylene; and PVC: poly(vinyl chloride)

Fabrication of PDMS Stamps

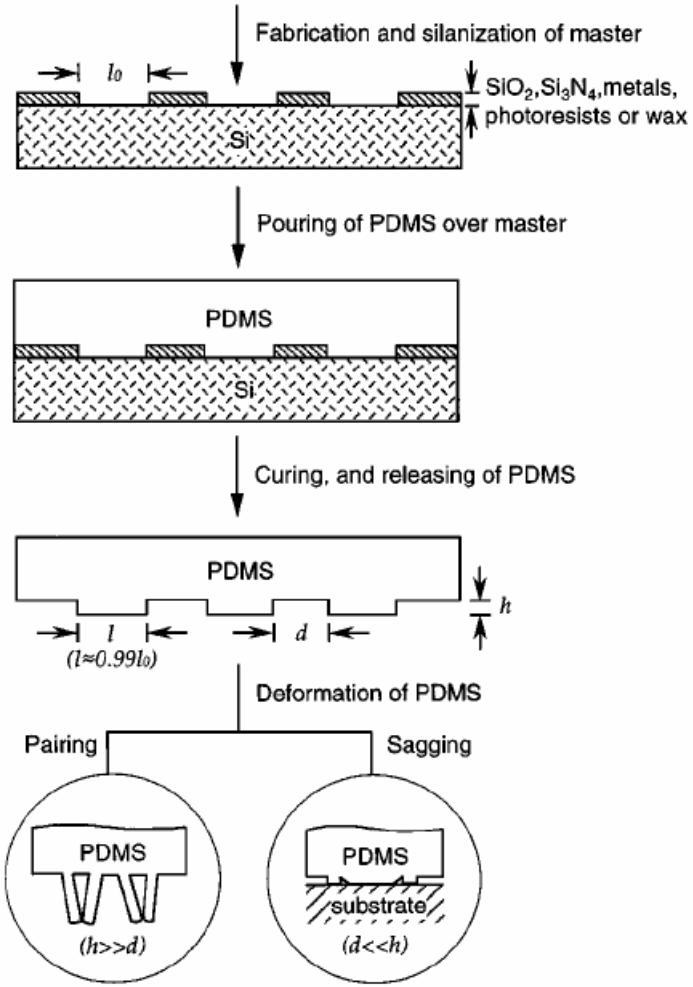

Figure 1 Schematic illustration of the procedure for fabricating PDMS stamps from a master having relief structures on its surface.

Printing Schemes

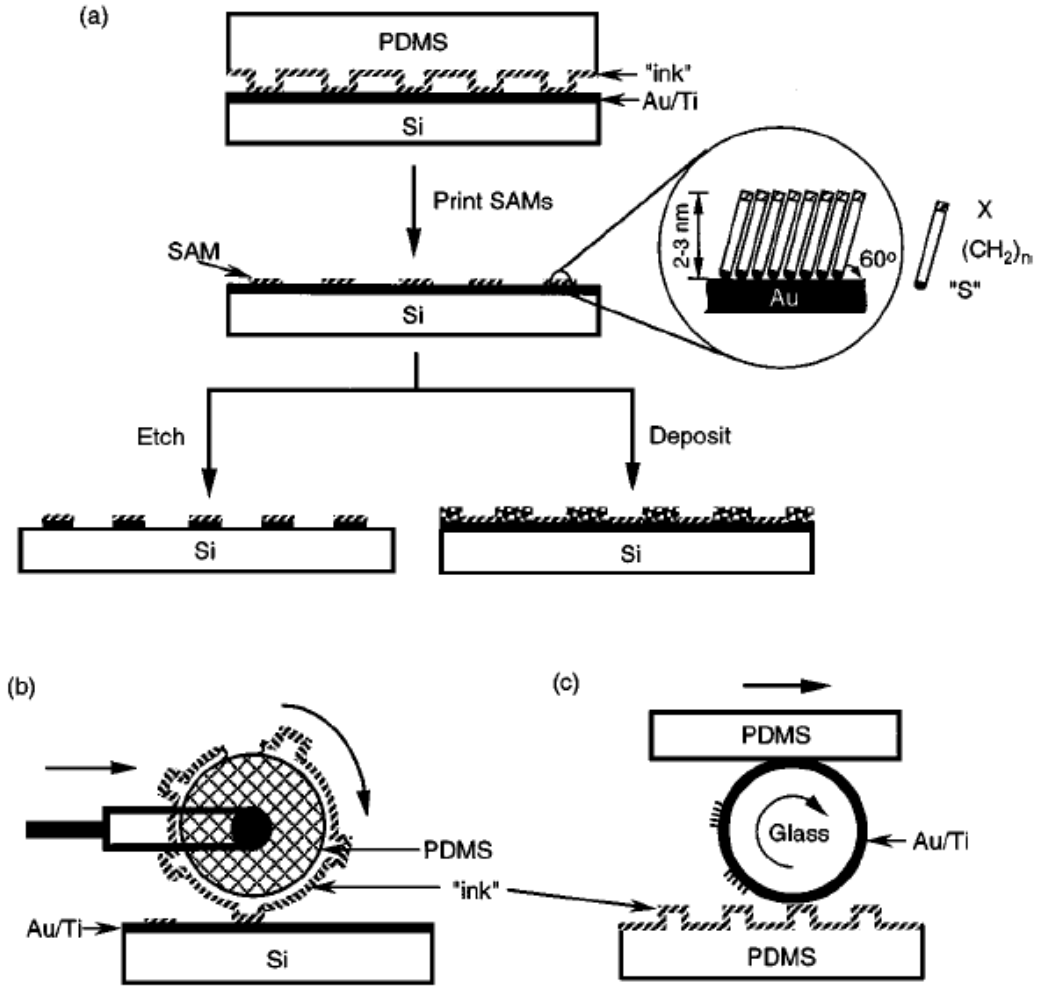

Figure 2 Schematic procedures for μCP of hexadecanethiol (HDT) on the surface of gold: (*a*) printing on a planar surface with a planar stamp (21), (*b*) printing on a planar surface over large areas with a rolling stamp (128), and (*c*) printing on a nonplanar surface with a planar stamp (174).

Printing Results

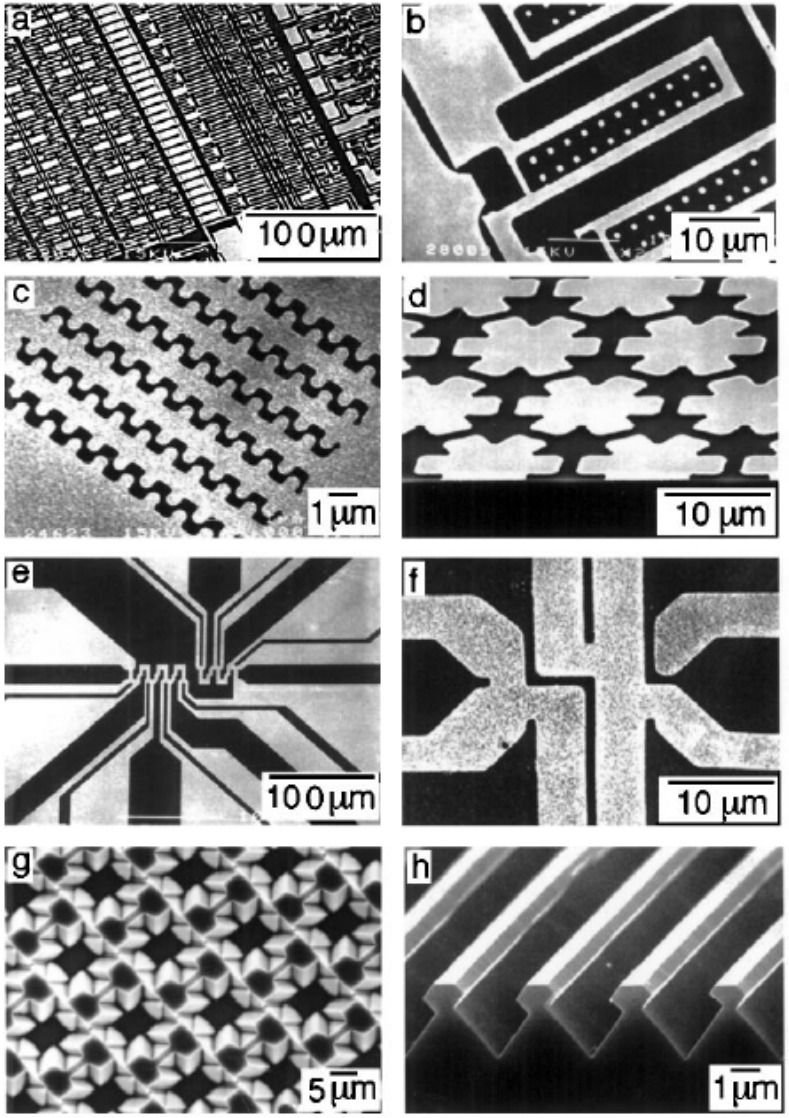

Figure 3 Scanning electron microscopy (SEM) images of test patterns of silver (*a–c*, 50 nm thick; *d*, 200 nm thick), gold (*e*, 20 nm thick), and copper (*f*, 50 nm thick) that were fabricated using μCP with HDT, followed by wet chemical etching. The patterns in (*a*) and (*b*) were printed with rolling stamps (128); the patterns in (*c–f*) were printed with planar stamps (113, 116, 126). The bright regions are metals; the dark regions are Si/SiO_2 exposed where the etchant has removed the unprotected metals. (*g,h*) SEM images of silicon structures fabricated by anisotropic etching of Si(100), with patterned structures of silver or gold as resists (44, 133). The structure in (*h*) was generated using a combination of shadow evaporation and anisotropic etching of Si⟨100⟩.

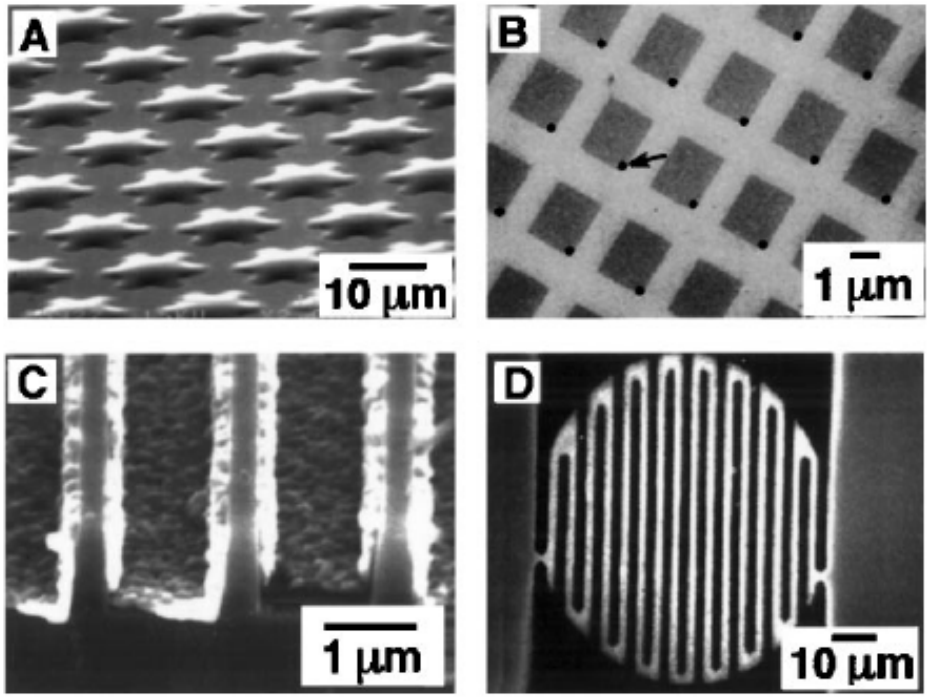

Figure 4 Selective wetting, nucleation, and deposition with patterned SAMs as templates: (*a*) An SEM image of microstructures of polyurethane (PU) assembled using selective dewetting (35). (*b*) An SEM image of microdots of $CuSO_4$ (*arrow*) formed by selective dewetting and crystallization (141). The dark squares are SAMs terminated in -COOH groups; the light grids are SAMs terminated in $-CH_3$ groups. (*c*) An SEM image of microstructures of Cu (*light*) formed in Si microtrenches using selective CVD (142). (*d*) An SEM image of microstructures of $LiNbO_3$ (*light*) on Si/SiO_2 (*dark*) produced using selective CVD (144).

Variations

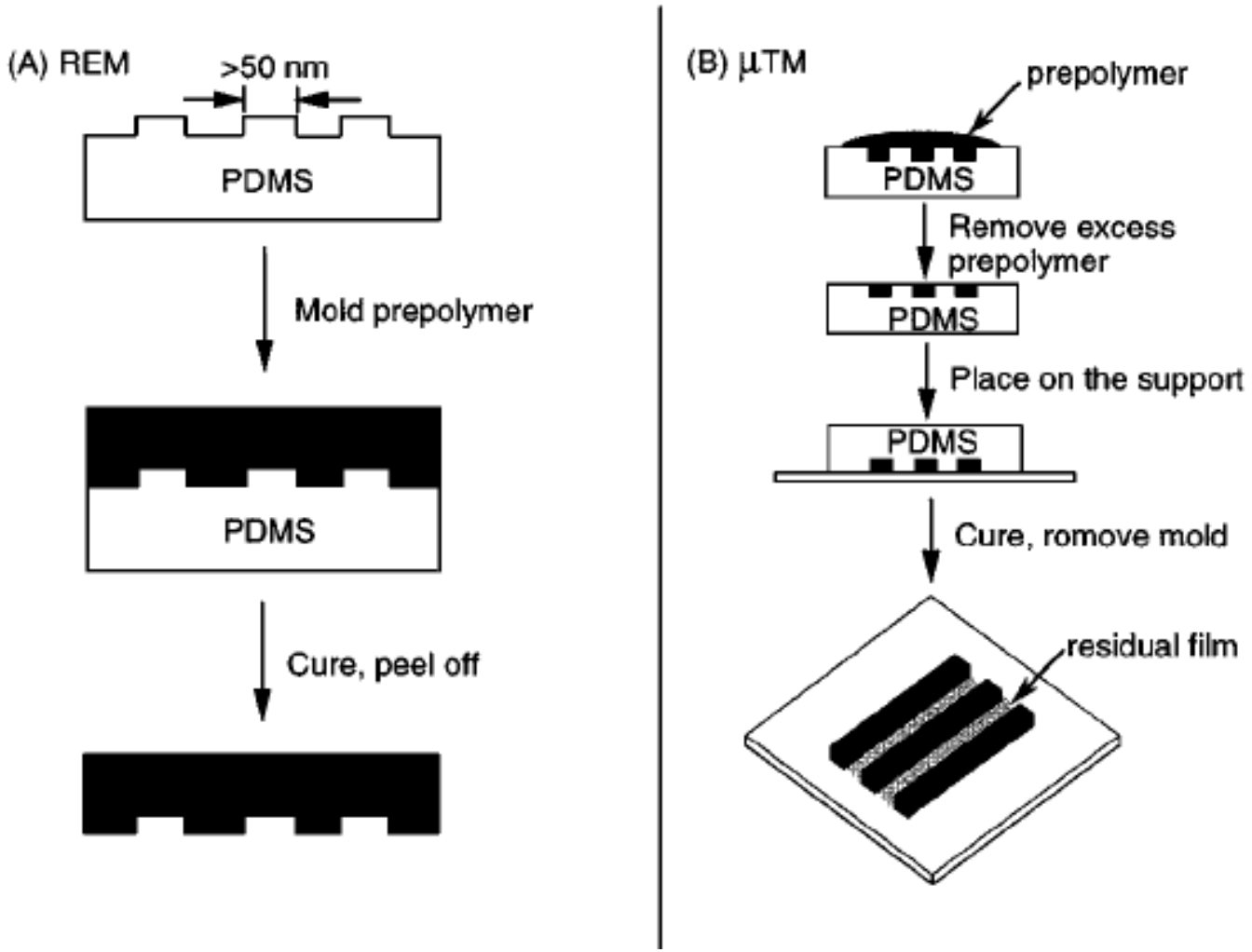
(A) REM
>50 nm
PDMS
Mold prepolymer
PDMS
Cure, peel off
(B) μTM
prepolymer
PDMS
Remove excess prepolymer
PDMS
Place on the support
PDMS
Cure, romove mold
residual film

Variations

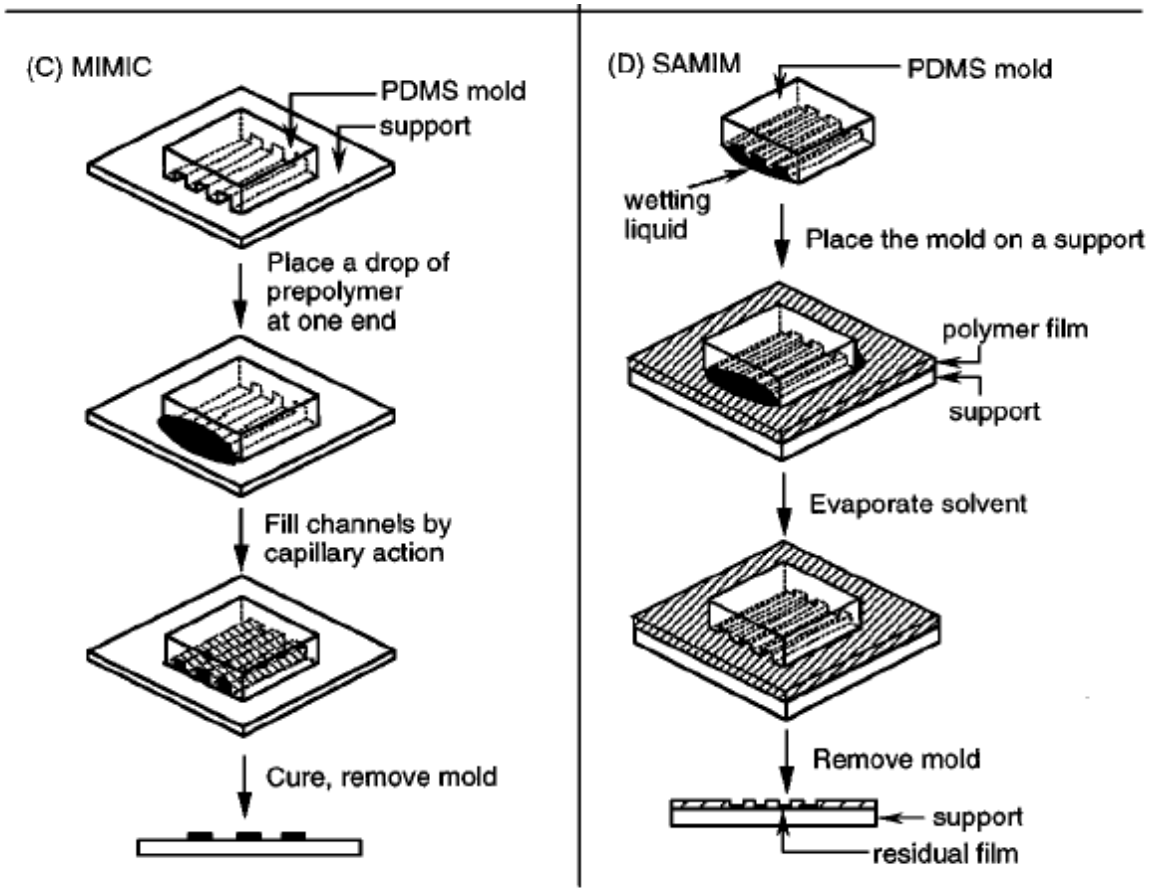

Figure 5 Schematic illustration of procedures for (*a*) replica molding (REM), (*b*) microtransfer molding (μTM), (*c*) micromolding in capillaries (MIMIC), and (*d*) solvent-assisted micromolding (SAMIM).

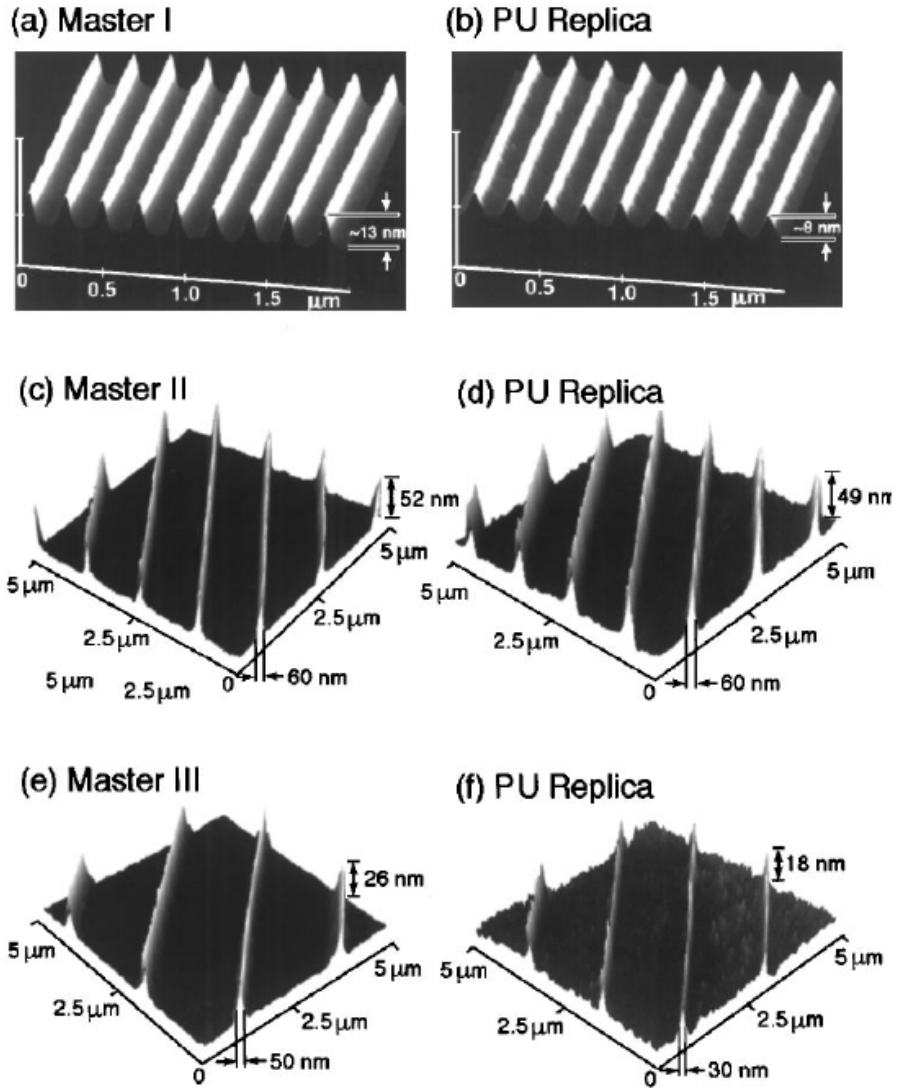

Figure 6 (*a,b*) Atomic force microscopy (AFM) images of Cr structures on a master, and a PU replica prepared from a PDMS mold cast from this master (153). (*c,d*) AFM images of Au structures on another master, and a PU replica produced from a PDMS mold cast from this master. (*e,f*) AFM images of Au structures on a third master, and a PU replica fabricated from a PDMS mold (cast from this master) while this mold was mechanically deformed by bending in a manner that generated narrower lines.

REM

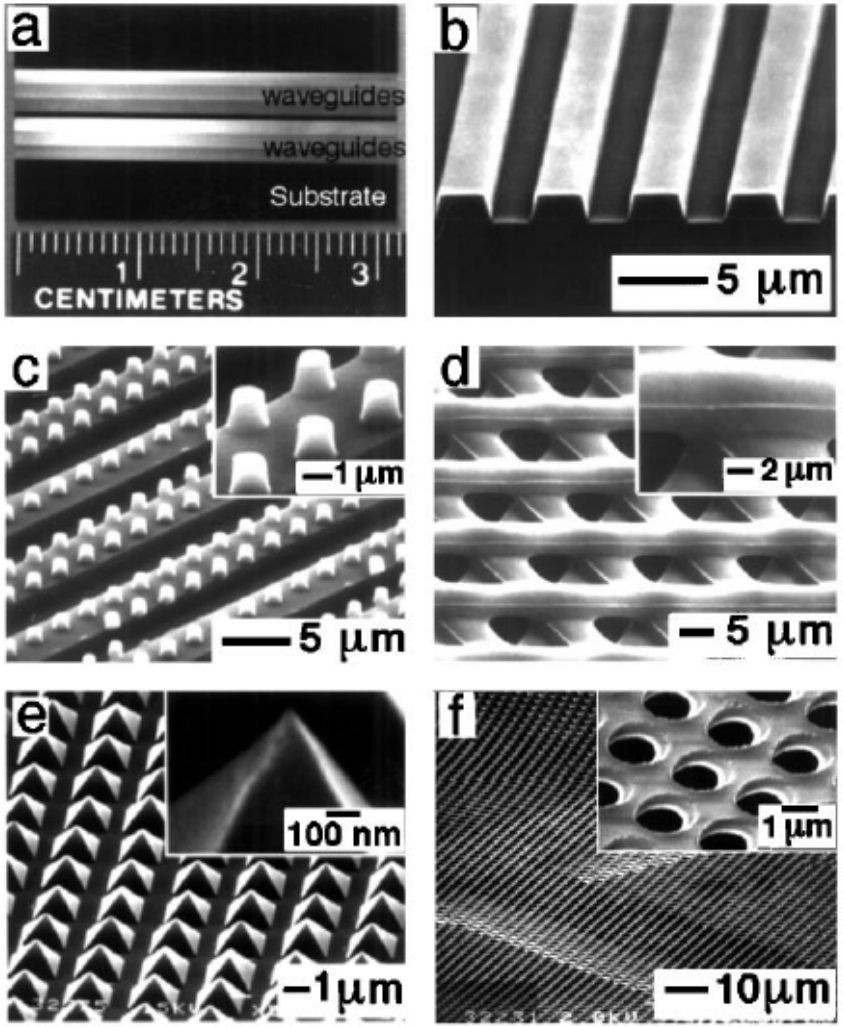

Figure 7 Polymeric microstructures fabricated using μTM (23). (*a*) A photograph of arrays of 3-cm long waveguides of PU fabricated on Si/SiO_2. The waveguides have different lateral dimensions and are separated by different spacing. (*b*) An SEM image of the ends of the waveguides. (*c*) An SEM image of an array of isolated microcylinders of epoxy on 5-μm lines of epoxy, supported on a glass slide. (*d*) An SEM image of a three-layer structure on a glass slide made from a thermally curable epoxy. (*e,f*) SEM images of microstructures of glasses fabricated by molding with sol-gel materials, followed by thermal consolidation.

μTM

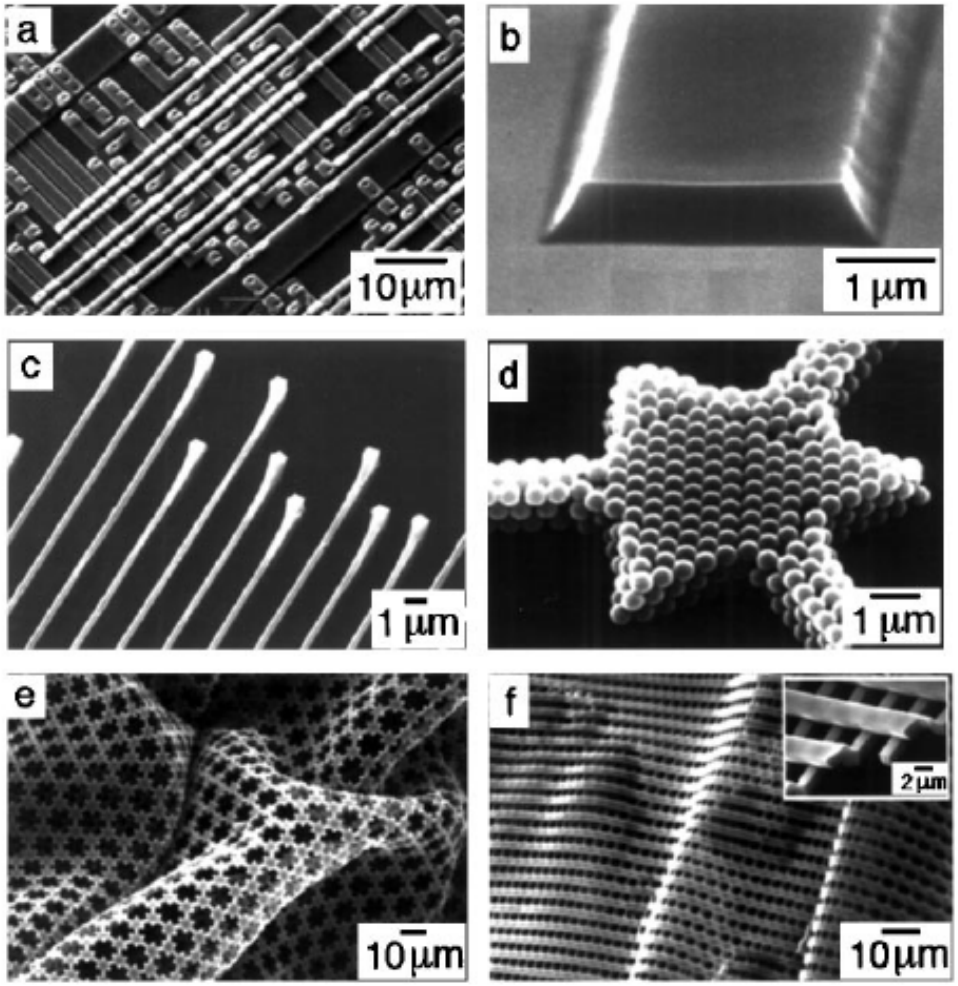

MIMIC

Figure 8 SEM images of microstructures of various materials fabricated using MIMIC (158, 159). (*a*) An SEM image of quasi-three-dimensional structures of PU formed on Si/SiO_2. (*b–d*) SEM images of patterned microstructures of polyaniline emeraldine HCl salt, zirconia (ZrO_2), and polystyrene beads, respectively, that were fabricated from their solutions or suspensions using MIMIC. (*e,f*) SEM images of free-standing microstructured membranes of polyurethane. The buckling occurred during sample preparation; the absence of fractures demonstrates their strength.

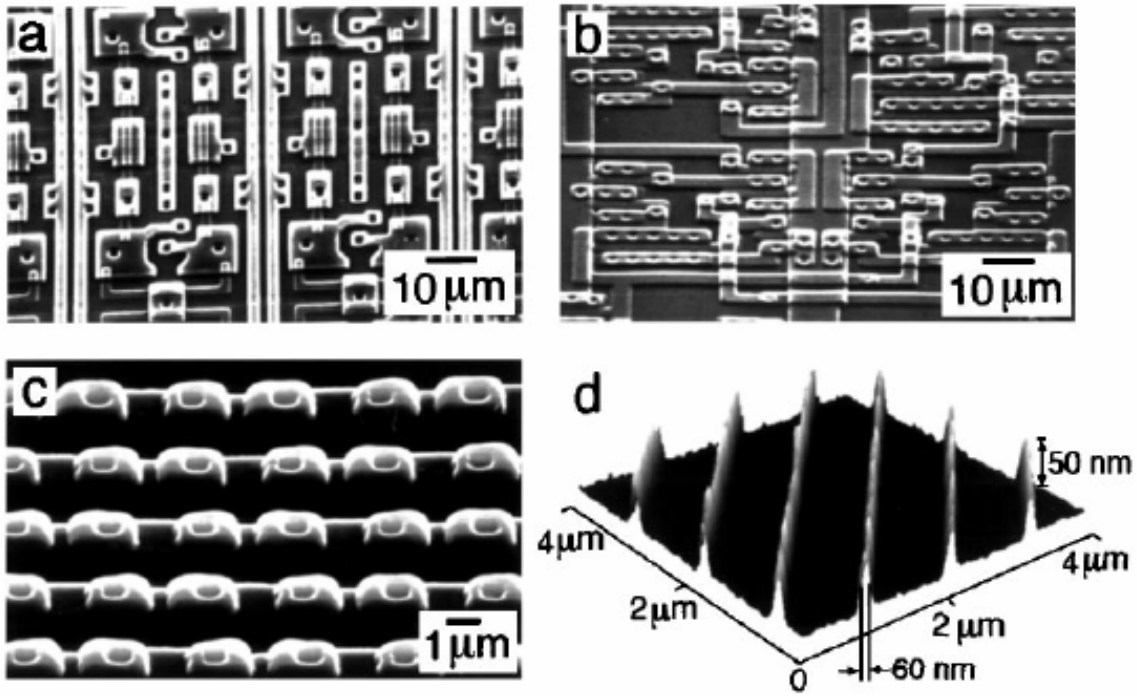

SAMIM

Figure 9 SEM and AFM images of polymeric microstructures fabricated using SAMIM (25). (*a–c*) SEM images of quasi-three-dimensional structures in photoresist (Microposit 1805, Shipley; ~1.6 μm thick) spin-coated on Si/SiO_2, polystyrene (PS, Goodfellow; 2.0 μm thick), and ABS (Goodfellow; 0.85 μm thick), respectively. (*d*) An AFM image of nanostructures in a thin (~0.4 mm thick) film of Microposit 1805 spin-coated on Si/SiO_2. The solvent we used was ethanol for the photoresist and acetone for PS and ABS.

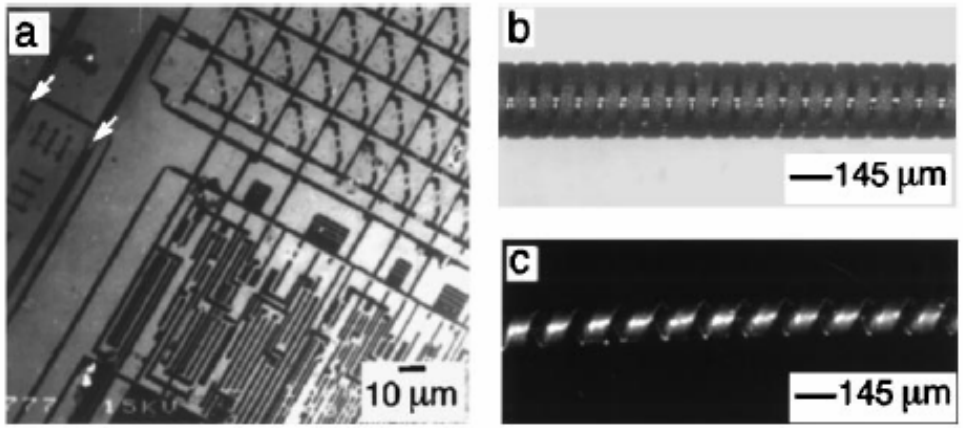

Figure 10 (*a*) The SEM image of test patterns of Au on the surface of a capillary that were fabricated using μCP with HDT, followed by selective etching in an aqueous KCN solution saturated with O_2 (174). The arrows indicate two defects caused by sagging. (*b,c*) Optical micrographs of a microtransformer and a micro-spring fabricated by μCP with HDT on silver (coated on the capillaries), followed by selective etching of silver and electroplating of (*c*) nickel and (*d*) copper (176, 178).

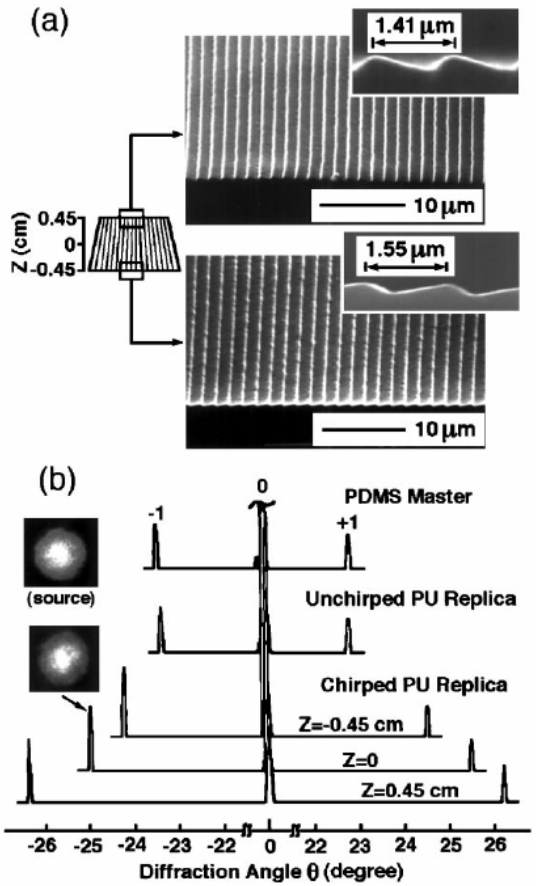

Figure 11 (*a,b*) Cross-sectional SEM images of selective regions of a planar, chirped, and blazed PU replica grating that was fabricated by molding against a PDMS mold while it was compressed asymmetrically (22). The PDMS mold was prepared by casting against a commercial blazed diffraction grating. (*c*) Diffraction patterns from the PDMS mold, its PU replica, and the chirped PU grating. A He-Ne laser ($\Lambda = 632.8$ nm) was used.

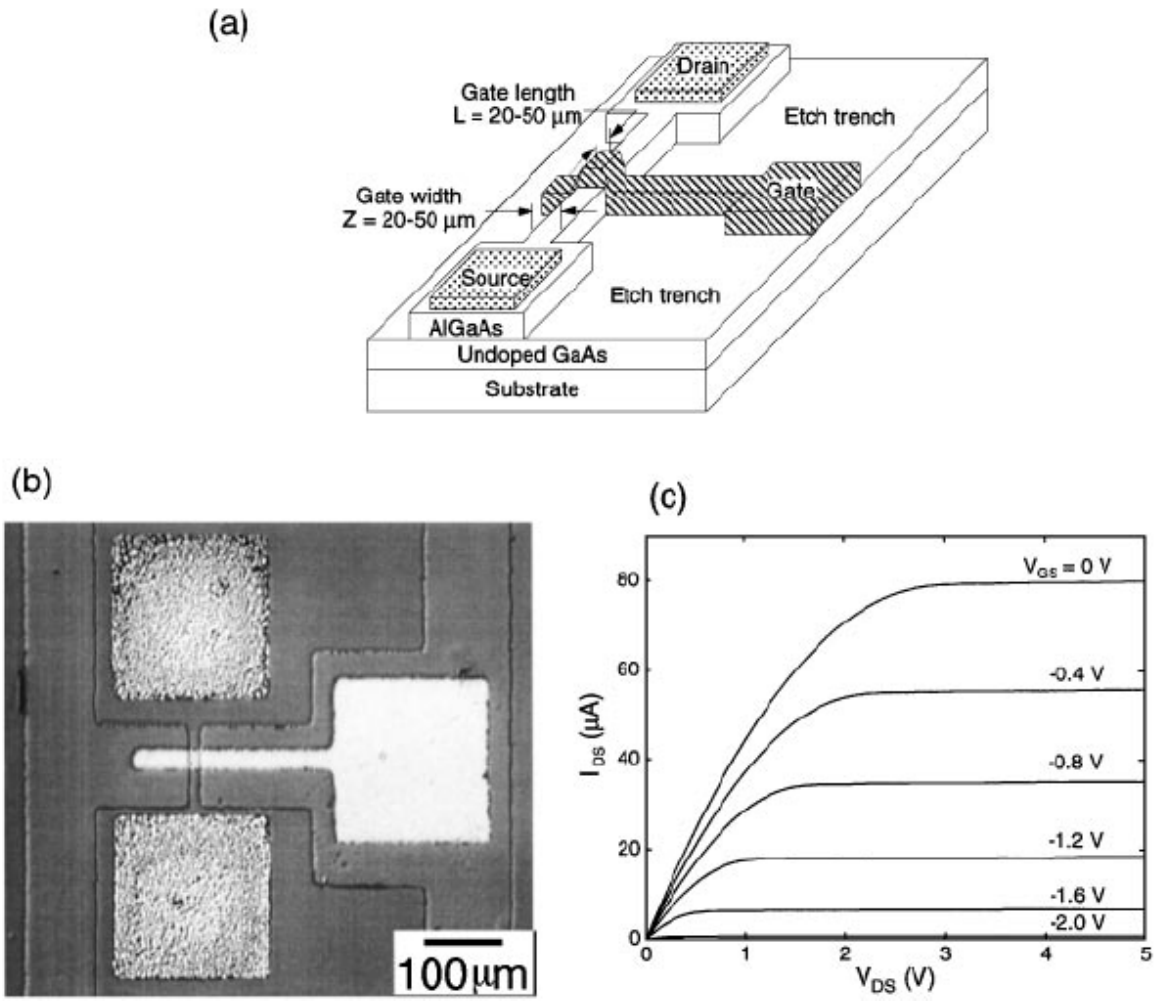

Figure 12 (*a*) Schematic diagram of a GaAs/AlGaAs FET. (*b*) Optical micrograph of a GaAs/AlGaAs FET ($L = 26$ μm and $Z = 16$ μm) fabricated using MIMIC (182). (*c*) The performance of a representative GaAs/AlGaAs FET fabricated using this procedure.

Printing Patterns of Proteins

André Bernard,[†,‡] Emmanuel Delamarche,[†] Heinz Schmid,[†] Bruno Michel,[†] Hans Rudolf Bosshard,[‡] and Hans Biebuyck*[,†]

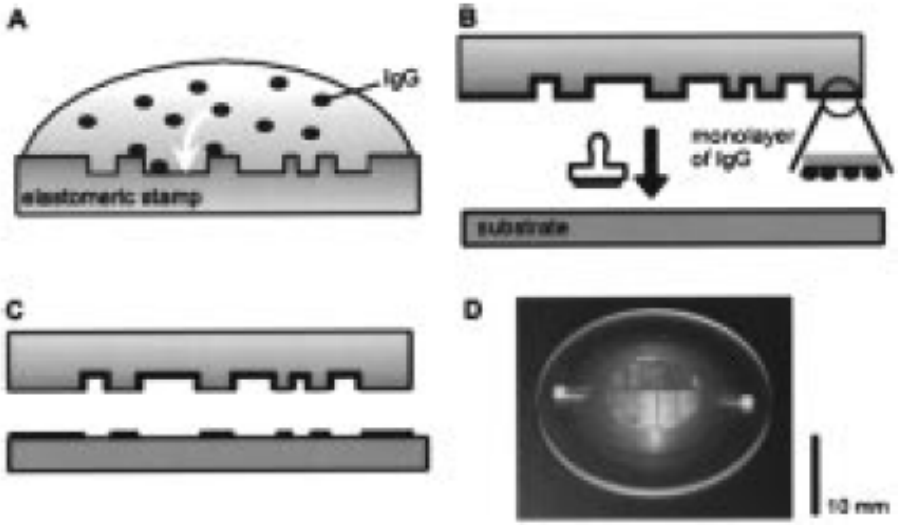

Figure 1. Procedure for directly patterning proteins on a substrate using elastomeric stamps. The stamp is fashioned by molding it from a master having a series of surface reliefs that will define areas of contact between the stamp and a substrate. (a) Equilibration of the surface of the stamp with a buffered solution of protein results, after a thorough rinsing in buffer and drying of the stamp under a stream of nitrogen, in (b) a monolayer of IgG on its surface. (c) Placement of the stamp under its own weight on a substrate and its removal after ≈1 s leaves a monolayer of IgG on the substrate wherever contact occurred. (d) Example of a PDMS stamp supported on a rigid backplane (glass) to facilitate alignment. The PDMS layer was 100 μm thick and had a relief pattern approximately 1 μm deep (evidenced here by defracting ambient light).

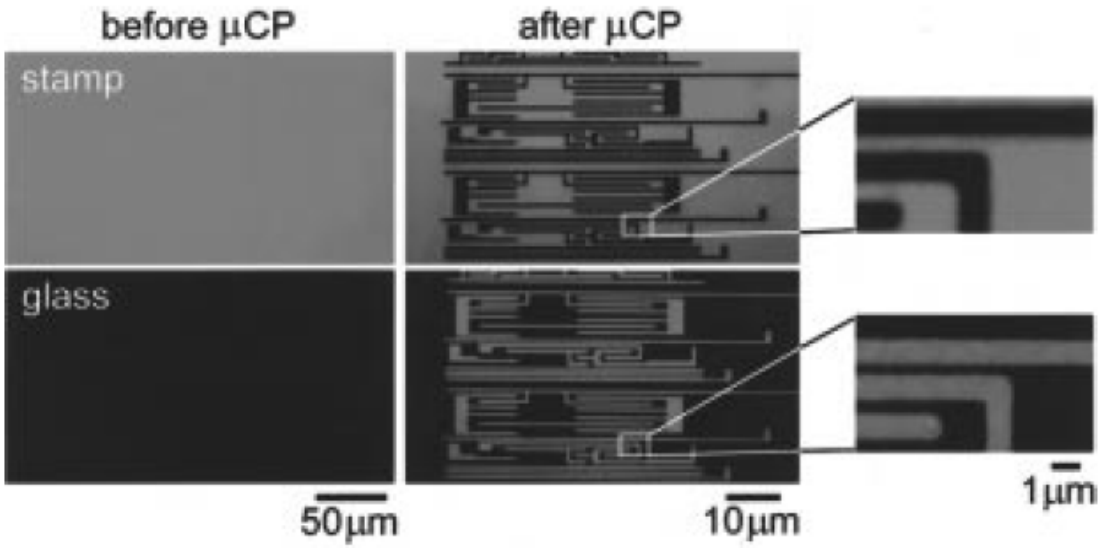

Figure 2. Monolayer of TRITC-tagged IgG transferred from a stamp to a glass substrate only where the two made contact. The fluorescence image (λ_{ex} = 552 nm) of the inked stamp appeared homogeneous prior to printing (top left image) with an intensity consistent with that for a monolayer of protein. The stamp had a series of patterned surface reliefs ≈300 nm deep, not visible in the image because tagged IgGs were present everywhere on the surface of the PDMS after the inking step (Figure 1a). Fluorescence was absent from raised regions in the same area of the stamp (top right image) after transfer of tagged IgGs from these areas by ≈1 s of contact between the stamp and a glass slide that initially had no emission at this wavelength (bottom left image). The complementary pattern in fluorescence appeared after printing on the glass slide (lower right image) that confirmed this transfer of tagged IgGs (a mirror operation was applied to this image to facilitate comparison with its upper counterpart). Quantifying the fluorescence signals showed that delivery of IgG from the stamp to the glass was >99% efficient in areas of their contact and that outside of these areas no changes to either surface occurred.

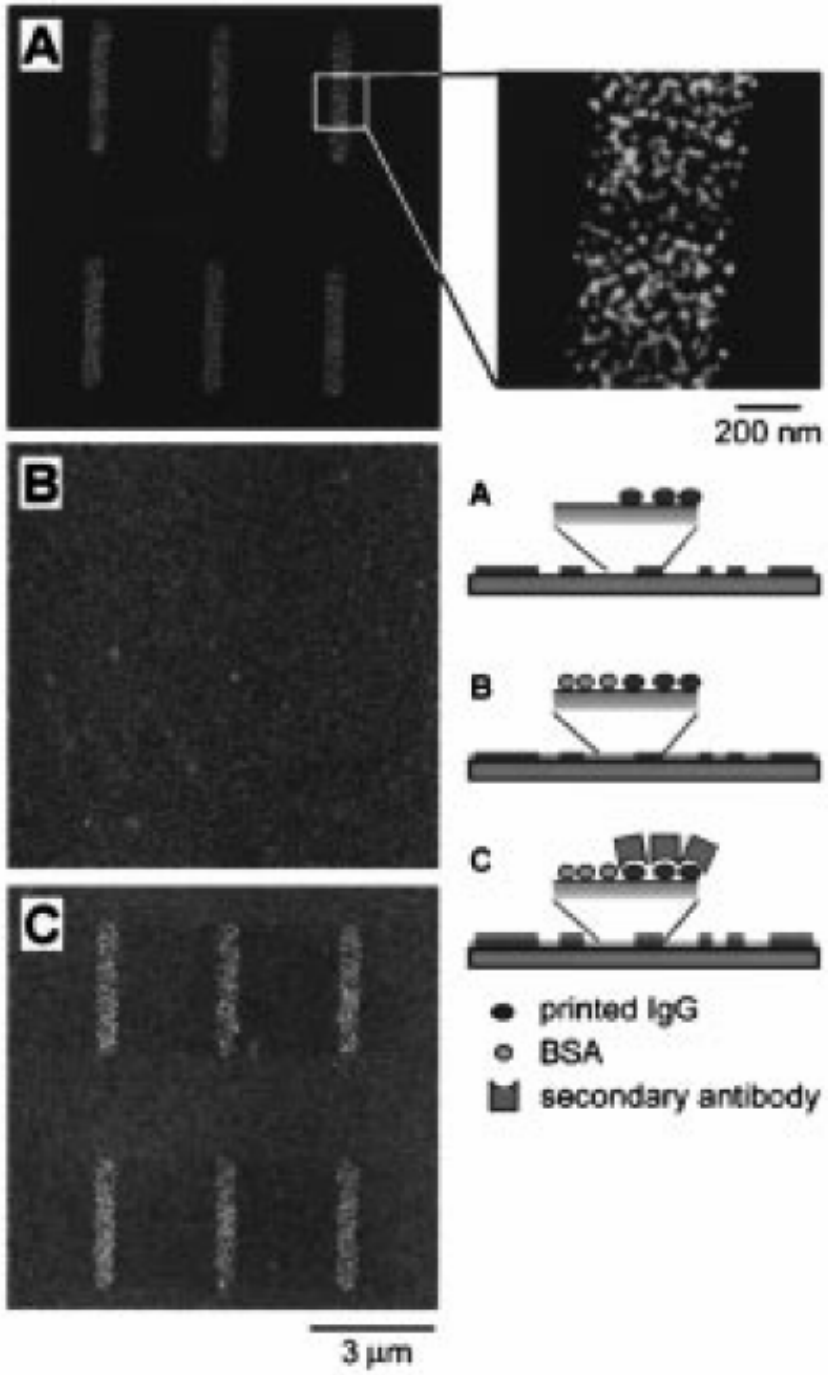

Figure 3. Detection by AFM of printed polyclonal chicken IgGs on hydrophobic silicon and their availability for specific recognition by secondary antibodies. (a) The image shows increases in height (3−4 nm) on the printed, and only the printed, regions of the substrate that are consistent with the localization of individual IgGs on the surface. (b) The same sample as in (a) was incubated in a solution of BSA to prevent nonspecific deposition of proteins on the substrate. The image, taken at the same location as in (a), shows a loss of topological contrast because BSA filled unoccupied sites on the surface. (c) The sample was removed from the AFM and incubated in a solution of anti-chicken antibodies. The sample was repositioned in the AFM to the area scanned in (a). The majority (≈70% by our count) of the printed IgGs remained sufficiently intact to allow their specific recognition by the secondary antibody. No significant presence of these secondary antibodies was evident anywhere outside the printed regions. The three schemes correlate the topographical information and the objects evident in the AFM images with the different types of proteins brought to the surface by the successive stamping, blocking, and recognition steps of the assay.

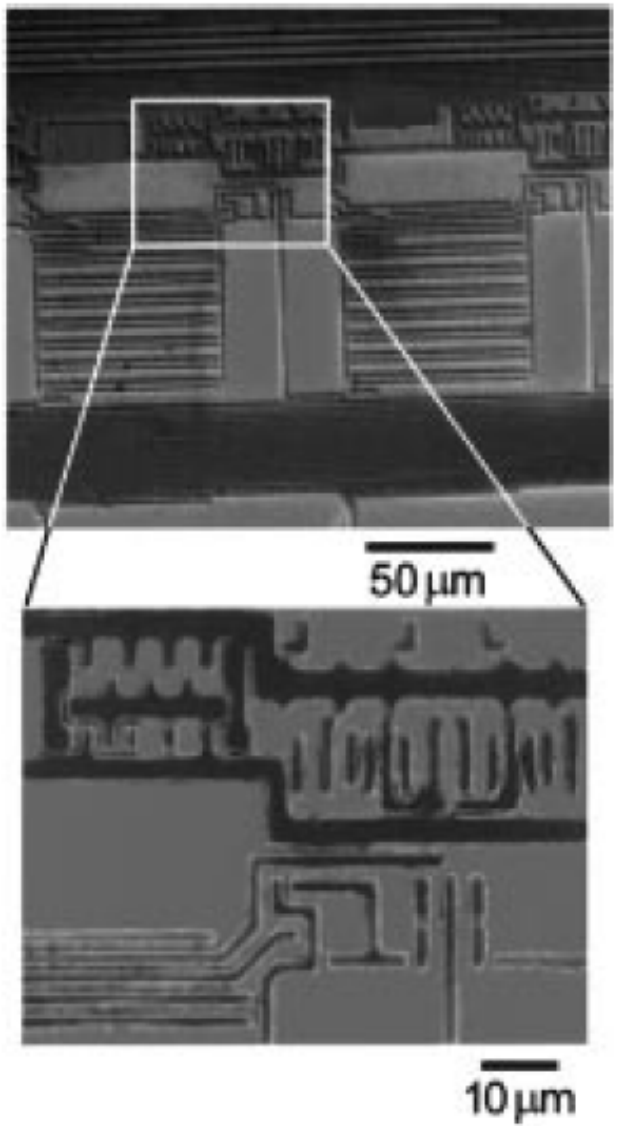

Figure 4. Secondary antibody recognition of printed or selectively adsorbed antibodies on a PS substrate showed similar levels of recognition using either preparation method. A stamp prepared with a polyclonal chicken IgG was used to print a pattern onto a PS culture dish. In a second step, monoclonal mouse IgGs were adsorbed from solution onto nonstamped areas of this polystyrene surface. The immunoassay was carried out with a solution of recognition IgGs: TRITC labeled anti-chicken IgGs (red), fluorescein isothiocyanate-conjugated antibody to mouse IgG (green), and R-phycoerythrin-conjugated antibody to bovine IgG (red-orange). Areas having stamped IgGs consequently appeared red and those with adsorbed IgG appeared green as a result of their specific recognition. No anti-bovine antibodies, providing a control for nonspecific deposition, were detected on the dish. Exchanging the identities of the stamped and solution-adsorbed IgG yielded the expected inversion in color in the image but did not otherwise affect the intensities of the fluorescence from either type of area (data not shown). Each color channel was collected independently (individual filters) so that emission resulting from cross-reactivity between the antibodies or their uncontrolled deposition would have been easily detected. All three images were then combined to form a digital composite of the result.

Table 1. Comparison of Printed and Solution-adsorbed Proteins

protein on substrate	assay of functionality	% rel performance stamped vs coated[a]
polyclonal chicken IgG	immuno staining	100
polyclonal rabbit IgG-TRITC	direct fluorescence	100
phosphatase (calf intestine)	*p*-nitrophenylphosphate (*p*NPP)	90
cytochrome c (horse heart)	ellipsometry	100
monoclonal mouse IgG	immuno staining	100
bovine serum albumin (BSA)	ellipsometry, ELISA-block	100
streptavidin, avidin	biotin-phosphatase/*p*NPP	80
protein A (staphylococcus aureus)	fluorescently labeled IgG	100
proteinase K (tritirachium album)	protein as substrate/Ninhydrin[b]	~50
peroxidase (horseradish)	H_2O_2, ABTS (chromogenic substrate)	60[c]
chymotrypsin (bovine pancreas)	*N*-benzoyl-L-tyrosinethylester/phenol red	70[d]
cell adhesion molecule (NgCAM)	cell attachment/cell growth[e]	~70

Langmuir **2002**, *18*, 519−523

Microcontact Printing of Proteins on Mixed Self-Assembled Monolayers

John L. Tan, Joe Tien, and Christopher S. Chen*

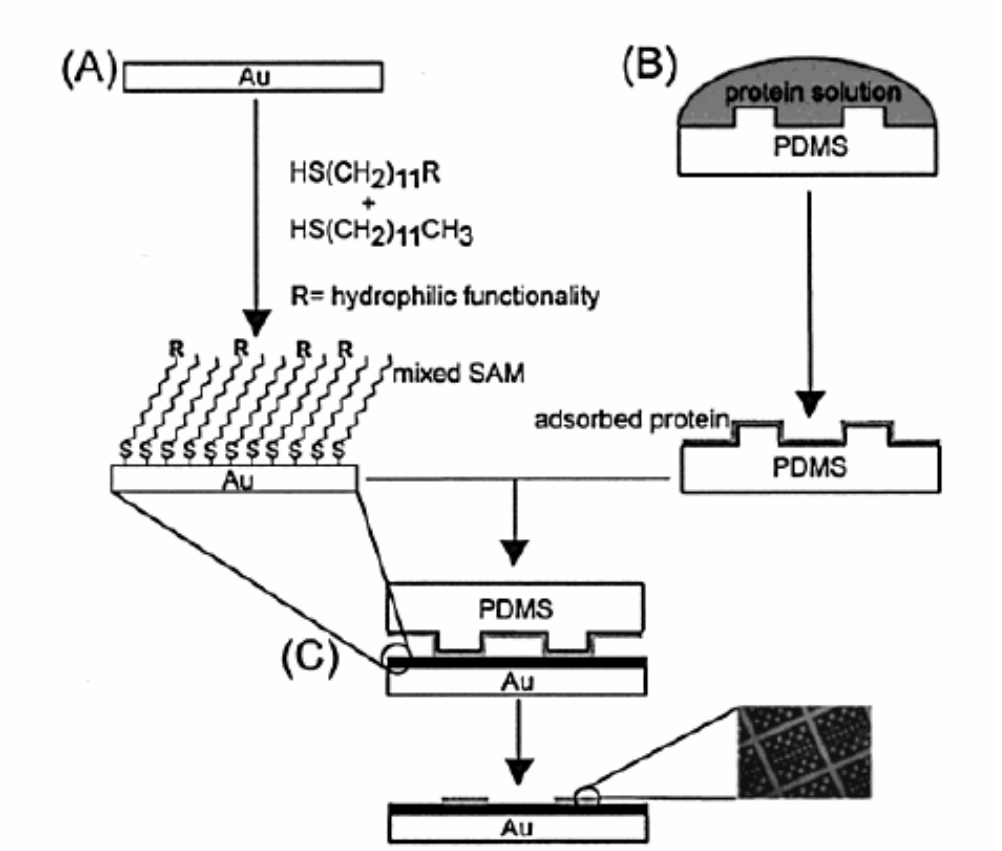

Figure 1. (A) Schematic of the formation of a two-component mixed SAM, (B) adsorption of proteins onto a PDMS stamp, and (C) μCP of protein from the stamp onto the mixed SAM with a sample micrograph of fluorescently labeled protein printed onto a 100% COOH SAM substrate.

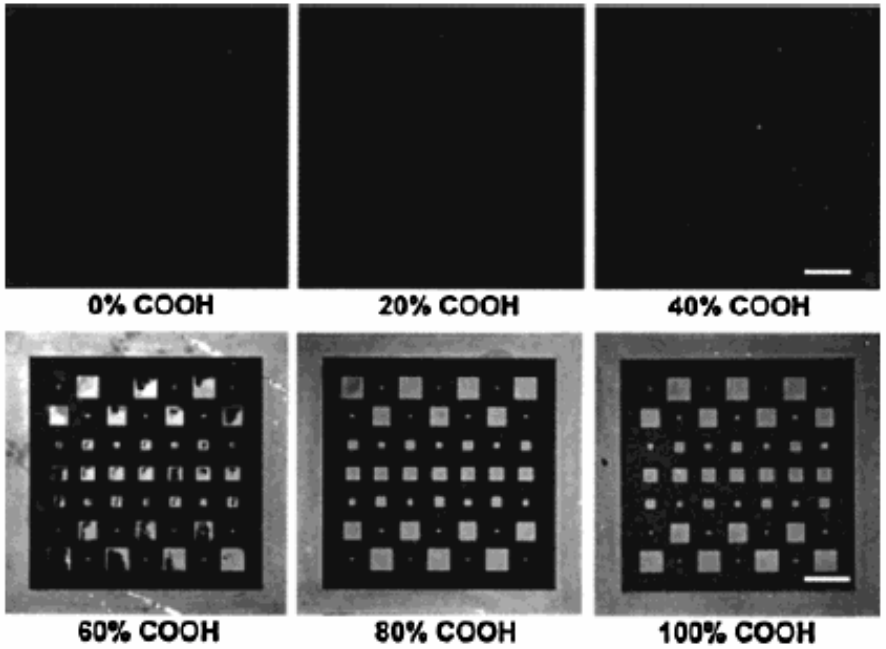

Figure 2. Micrographs of fluorescently labeled protein that was printed onto SAMs of various $-COOH/-CH_3$ compositions. Each image is a representative image from experiments repeated a minimum of three times with similar results. The scale bar represents 100 μm.

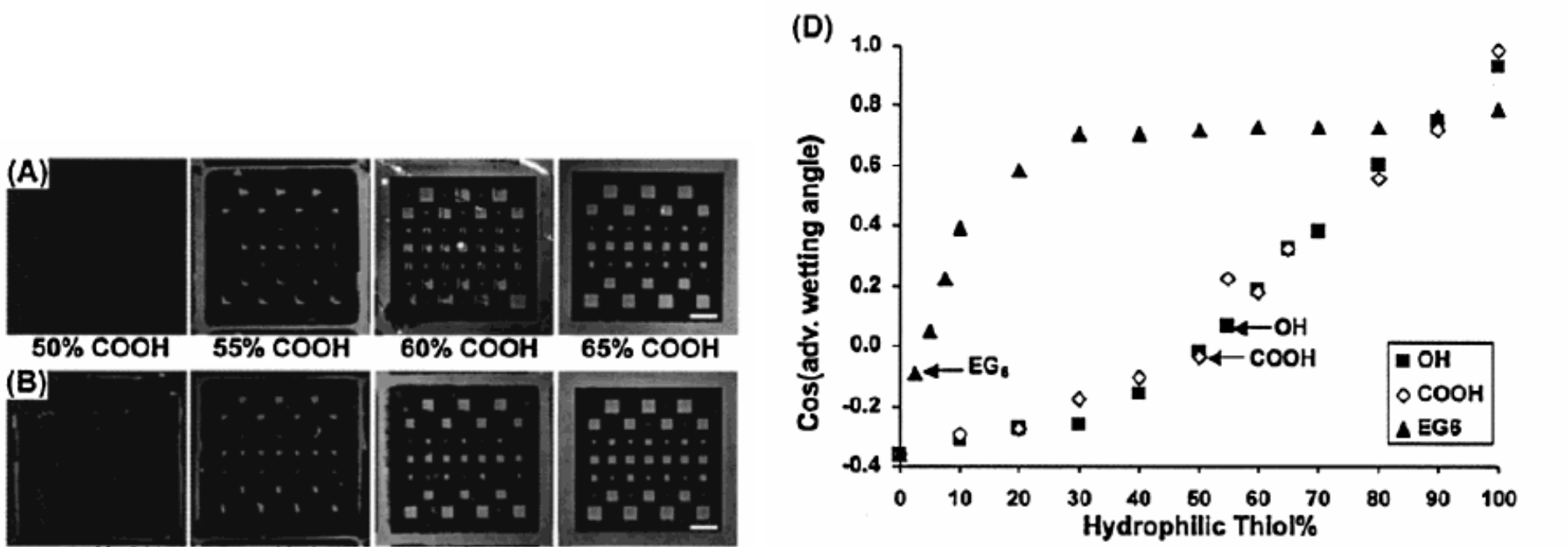

Figure 3. Printing of proteins on three different types of mixed SAMs. (A–C) Micrographs of fluorescently labeled protein printed onto mixed SAMs of alkanethiol presenting $-CH_3$ and (A) $-COOH$, (B) $-OH$, and (C) $-EG_6OH$ functionalities. Each image is a representative image from experiments repeated a minimum of three times with similar results. The scale bars represent 100 μm. (D) Plot of the cosine of the advancing water contact angle against the percentage of polar functionalities for each of the three types of mixed SAMs. Each data point plotted is the average of a minimum of three measurements taken on two separately prepared SAM substrates. Labeled arrows mark the contact angles of the minimum percentage of the indicated SAM on which we observed any protein transfer onto each type of mixed SAMs.

Table 1. Advancing Contact Angles of Deionized Water on the Silanized Surface of the Stamp and on Transition Substrates[a]

surface functionality of PDMS stamp	θ_{stamp} (deg)	$\%COOH_1$	θ_1 (deg)	$\%COOH_2$	θ_2 (deg)
untreated	112	55	92	65	71
$-CF_3$	120	0	111	20	106
$-NH_2$	28	80	56	90	44

[a] θ_{stamp} refers to advancing contact angles of water on the indicated PDMS surface. $\%COOH_1$ indicates the minimum percentage of COOH SAM where any transfer of protein was observed from the corresponding stamp, and θ_1 refers to the advancing angle on the SAM. $\%COOH_2$ indicates the minimum percentage of COOH SAM where the complete transfer of protein was observed, and θ_2 refers to the advancing angle on the SAM. Measurements were taken using deionized water in ambient conditions. For each contact angle listed, $n \geq 2$ and the standard deviation is $<3°$.

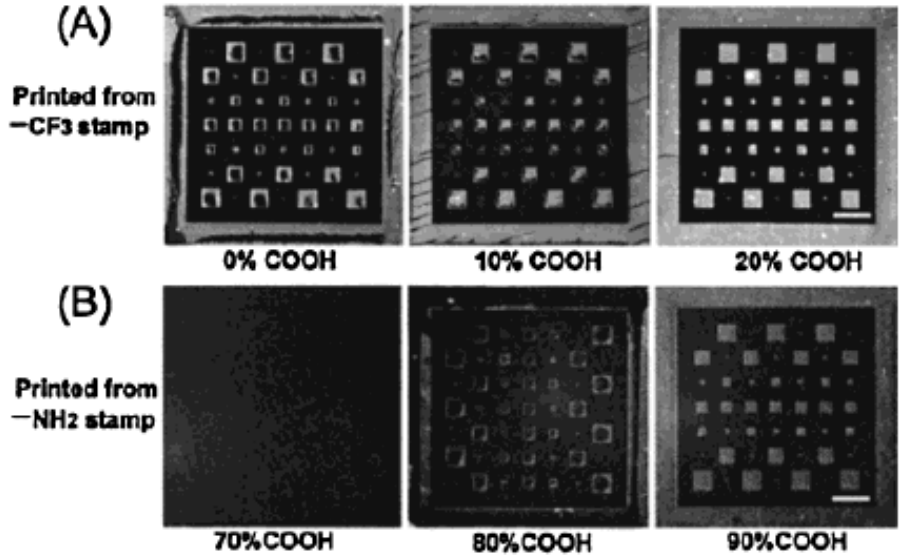

Figure 4. The role of the surface energy of the stamp on printing. Micrographs of fluorescently labeled protein printed onto the indicated percentage of COOH mixed SAM from (A) the $-CF_3$ functionalized stamp and (B) the $-NH_2$ functionalized stamp. We observed that less than a complete monolayer of protein adsorbed onto the $-NH_2$ functionalized stamp, which likely resulted from the reduced capacity of hydrophilic surfaces to adsorb protein (ref 27). To accommodate for the decreased fluorescence even in conditions that allow complete transfer of protein onto the substrate, we lengthened the exposure time for micrographs in (B) in comparison to all previously shown images. The scale bars represent 100 μm.

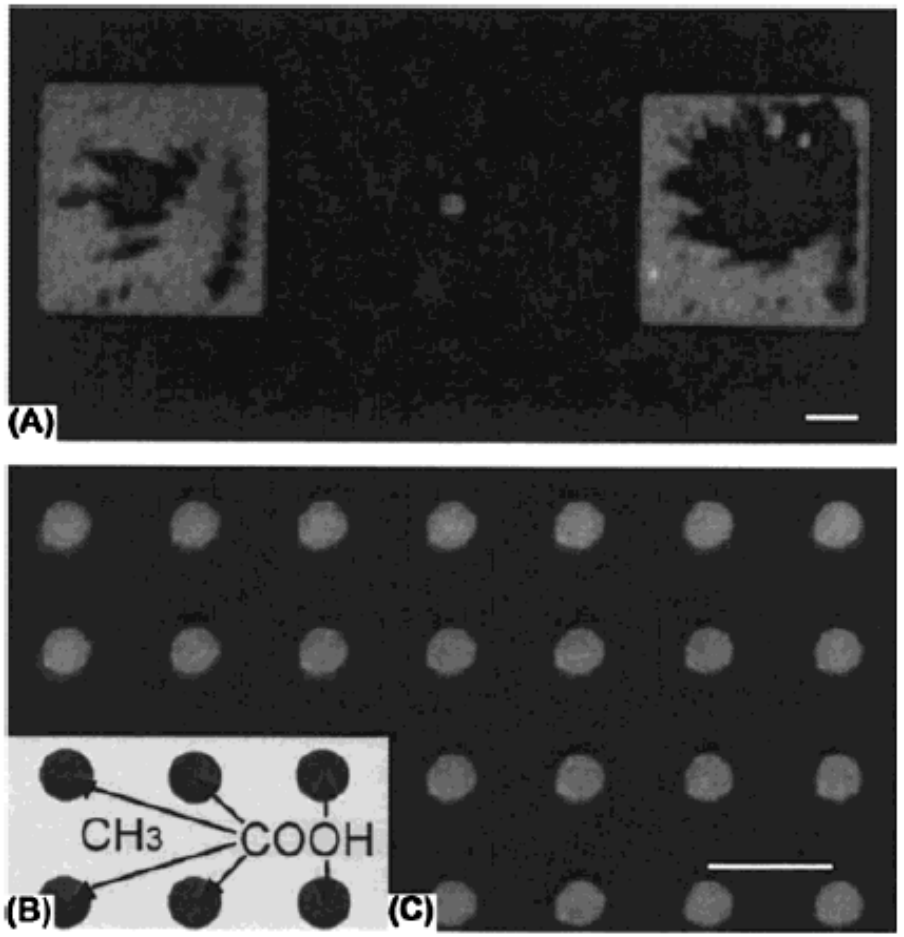

Figure 5. (A) Digitally magnified image of protein printed onto 60% COOH mixed SAMs, (B) schematic of the localization of COOH− and CH_3− terminated alkanethiols on a patterned SAM, and (C) representative image of proteins printed onto a patterned SAM from a flat unpatterned stamp. We observed similar results when a patterned stamp was used to μCP protein onto a patterned SAM. This image was captured on a higher magnification objective with a shorter exposure time than other images. The scale bars represent 10 μm.

Microcontact Printing of Proteins**

By *André Bernard*,* *Jean Philippe Renault*, *Bruno Michel*, *Hans Rudolf Bosshard*, and *Emmanuel Delamarche*

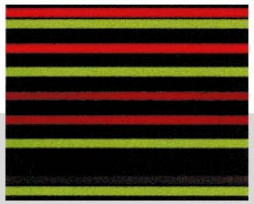

Adv. Mater. **2000**, *12*, No. 14, July 19

The direct patterning of biomolecules on a solid substrate can be achieved using microcontact printing, a method that has been very successfully adopted for the precise and gentle transfer of proteins and lipid bilayers from stamp to substrate in 1 s, without loss of biological activity. The image shown was produced by patterning 16 different proteins onto the polystyrene surface of a cell culture dish using a stamp inked by means of a microfluidic network.

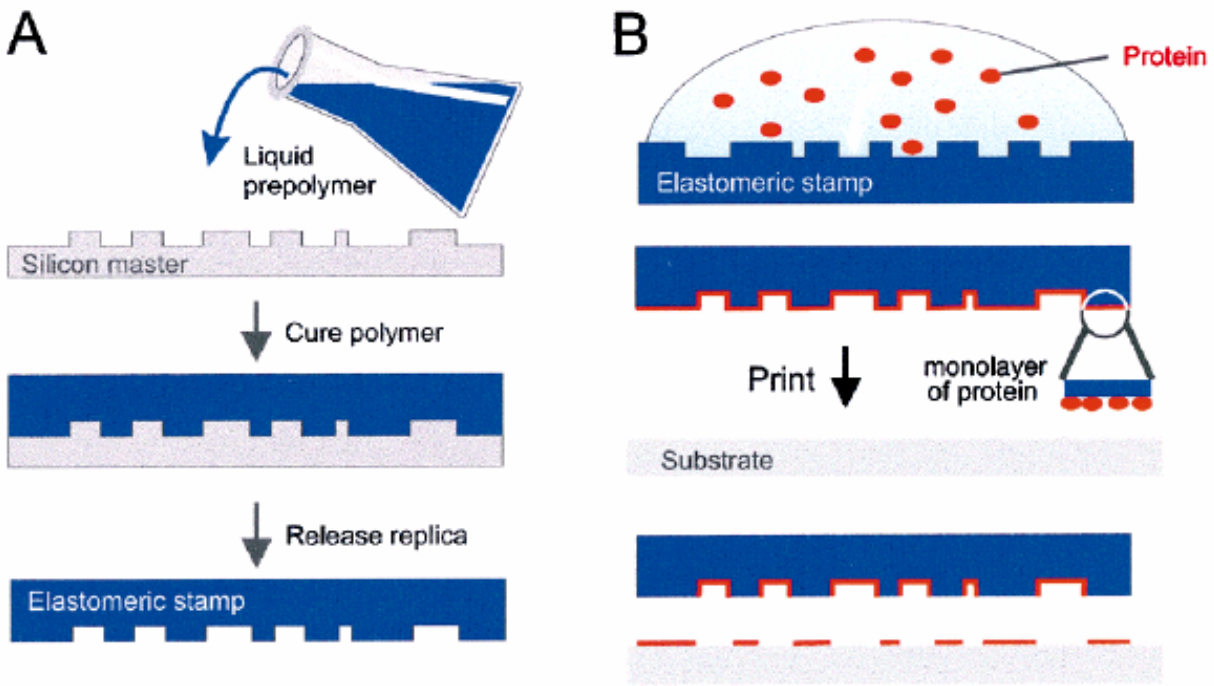

Fig. 1. A) Scheme of fabrication of a stamp and B) of its use in μCP. A conventionally fabricated master (usually from a Si wafer) is replicated by pouring liquid prepolymer of PDMS onto the master and then curing it. After its release, the stamp serves as the vehicle to transfer the "ink", in this case proteins, to a substrate upon brief contact. Transfer occurs only at the sites of conformal contact between stamp and substrate.

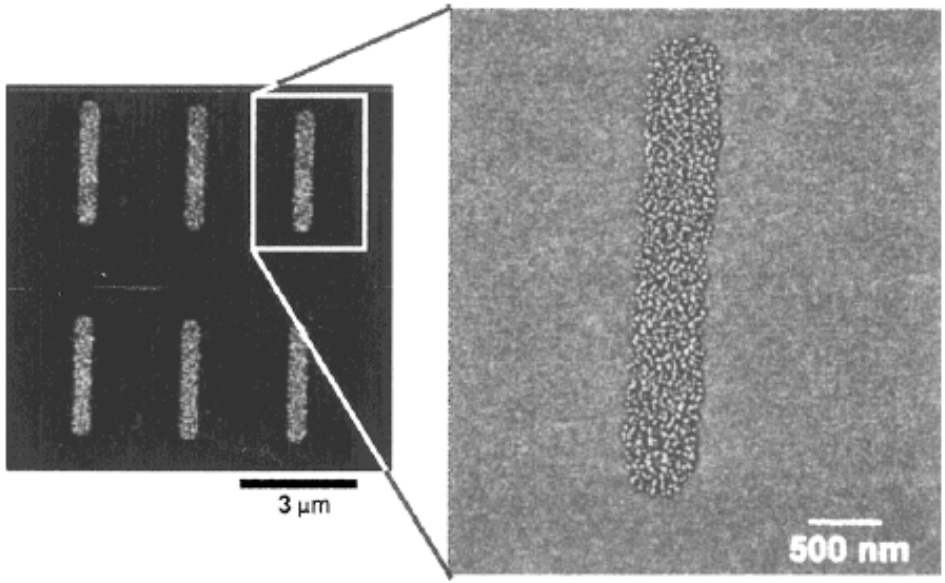

Fig. 2. AFM images (obtained in "tapping mode") of immunoglobulins G printed onto a Si wafer. The native oxide of the wafer was removed with 0.5 % HF for 15 s to render it hydrophobic. Each zone of contact comprises ~1500 printed antibodies, where each protein occupies ~150 nm^2 of the surface. The resolution and contrast of the protein pattern is striking.

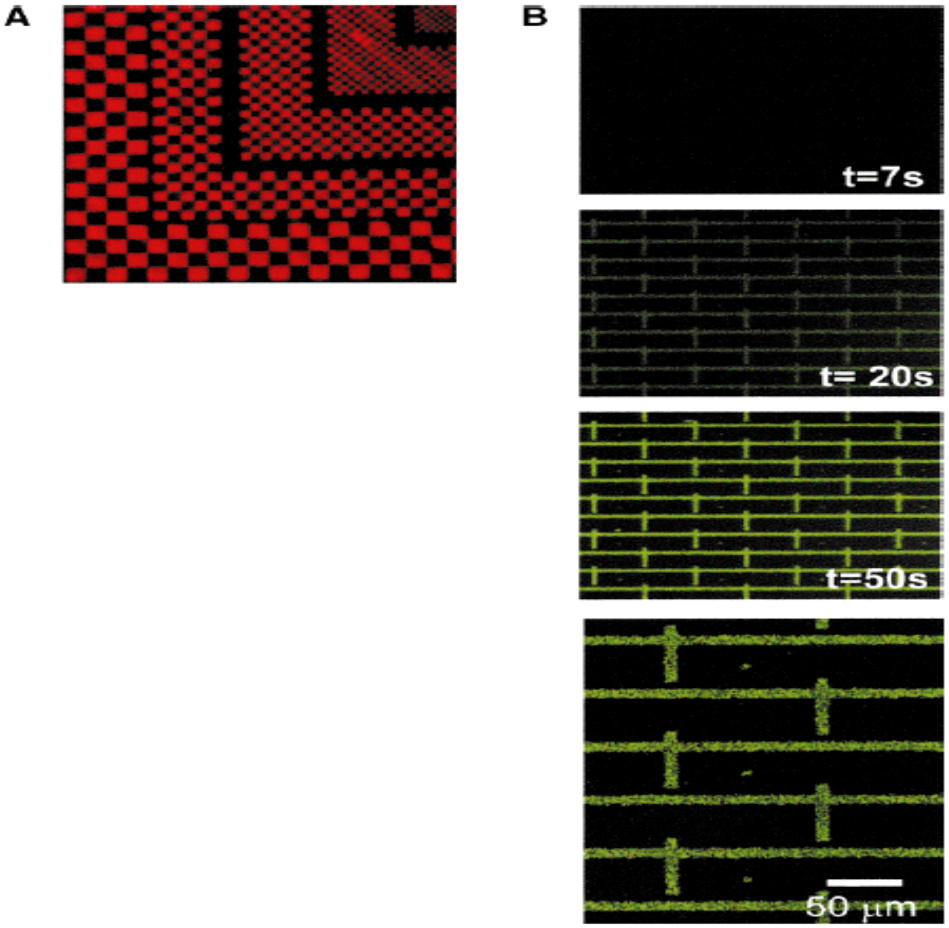

Fig. 3. Visualization and activity of microcontact-printed proteins. A) Fluorescence images of rhodamine-labeled antibodies patterned by μCP onto a glass slide. B) Time-resolved catalytic activity of a printed alkaline phosphatase converting a fluorogenic substrate into its insoluble product, which precipitates at the patterned sites of production.

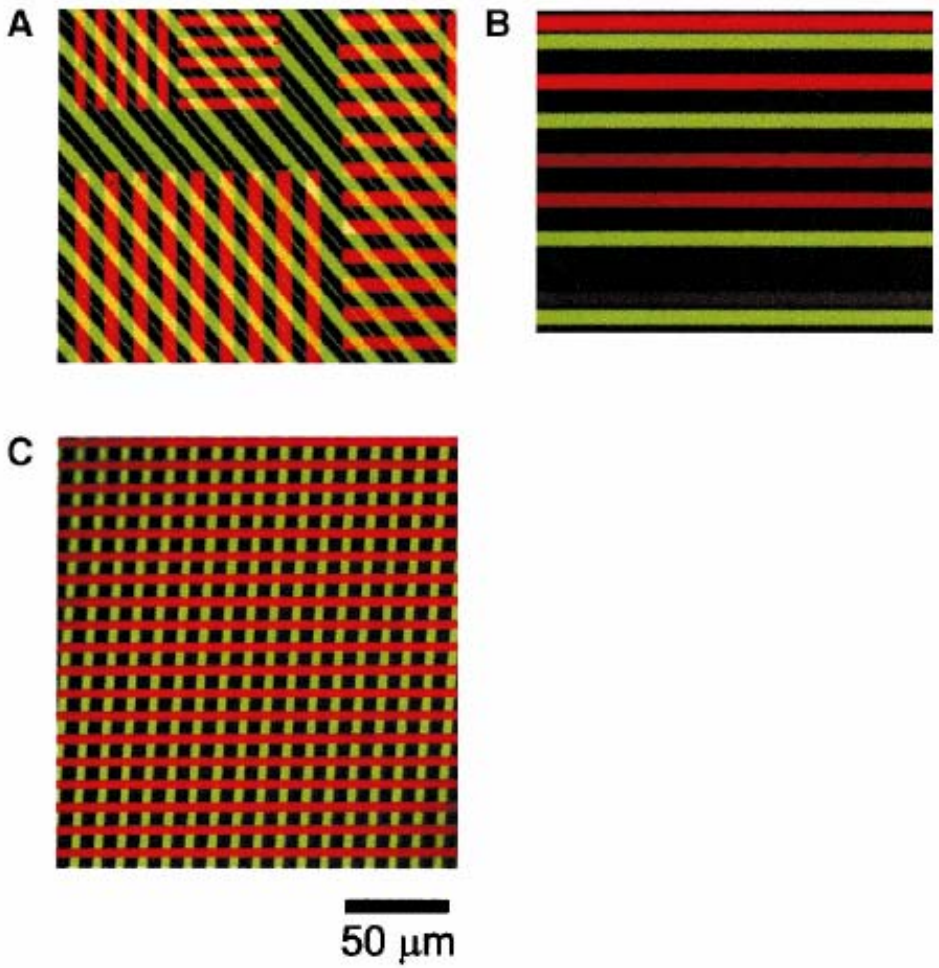

Fig. 4. Fluorescence images of microcontact printed proteins onto a substrate. A) Two different proteins have been subsequently printed onto the same glass substrate using different PDMS stamps. B) 16 different proteins (some of them without fluorescent label) were patterned onto the polystyrene surface of a cell culture dish using a stamp inked by means of a microfluidic network. C) Three different proteins simultaneously printed onto a glass slide by a flat stamp. The stamp was inked homogeneously with the first protein, then brought into contact with a patterned silicon surface. In the regions of contact, the proteins were transferred to the silicon (lift-off), opening up areas for subsequent protein adsorption onto the stamp. This procedure can be repeated using objects made of different materials such as silicon, glass, or plastic to lift-off patterns of proteins from the stamp.

Siloxane Polymers for High-Resolution, High-Accuracy Soft Lithography

H. Schmid and B. Michel*

Table 1. New Blends Prepared Using Different Vinyl and Hydrosilane Prepolymers

Vinyl-Terminated Polydimethylsiloxanes and Vinylmethylsiloxane−Dimethylsiloxane Copolymers			
M_c (D)	MW (D)	%	name
550	550	11	DMS-V03
770	770	7.9	DMS-V05
6000	6000	1.0	DMS-V21
9400	9400	0.5	DMS-V22
17200	17200	0.4	DMS-V25
28000	28000	0.22	DMS-V31
49500	49500	0.12	DMS-V35
7400	~30000	1	VDT-131
1644	~30000	4.5	VDT-431
987	~30000	7.5	VDT-731
512	>20000	12	VDT-954
<100	~1000	100	VMM-010
Methylhydrosilane−Dimethylsiloxane Copolymers			
ϕ	MW (D)	%	name
2	1950	6.5	HMS-071
4.3	1950	16.5	HMS-151
7.2	1950	27.5	HMS-301
7.4	1050	52.5	HMS-501
23	1950	100	HMS-991/PS-120

Table 2. Surface Hardness as a Function of Vinyl Ratio in the Prepolymer and Hydrosilane Ratio in the Cross-Linker[a]

%	wt % vinyl in prepolymer	M_c	surface hardness % of glass, H-to-vinyl ratio			compression modulus (N mm^{-2})	elong at break
			1.25	1.5	2		
wt % hydrosilane in cross-linker 6.5, $\phi = 2$, $M_{c_2} = 1950$ D	12	512	0.41	**0.44**	0.31	1.64 ± 0.03	8.6
	7.5	987	**0.51**	0.43	0.30	2.12 ± 0.12	6.7
	4.5	1644	**0.56**	0.40	0.30	1.81 ± 0.05	7.5
	1.0	7400	**0.16**	0.15	0.11	too soft	13.6
wt % hydrosilane in cross-linker 16.5, $\phi = 4.3$, $M_{c_2} = 1950$ D	12	512	**2.23**	1.61	1.89	7.81 ± 0.52	9.3
	7.5	987	**1.78**	1.43	1.00	3.91 ± 0.06	10.7
	4.5	1644	**1.00**	0.94	0.72	4.21 ± 0.06	10.1
	1.0	7400	0.22	**0.24**	0.2	0.60 ± 0.02	20.0
wt % hydrosilane in cross-linker 27.5, $\phi = 7.2$, $M_{c_2} = 1950$ D	12*	512	**2.04**	1.42	1.18	foam	foam
	7.5*	987	**2.59**	2.10	1.43	**8.97 ± 0.21**	**5.7**
	4.5	1644	1.51	**1.52**	1.24	6.51 ± 0.14	7.2
	1.0	7400	0.26	**0.28**	0.24	0.79 ± 0.02	18.4
wt % hydrosilane in cross-linker 52.5, $\phi = 7.4$, $M_{c_2} = 1050$ D	12*	512	foam	foam	foam	foam	foam
	7.5*	987	2.02	**2.77**	1.61	8.57 ± 0.12	8.7
	4.5	1644	1.15	**1.75**	1.40	4.67 ± 0.32	11.7
	1.0	7400	0.21	0.29	**0.31**	0.73 ± 0.07	28.4

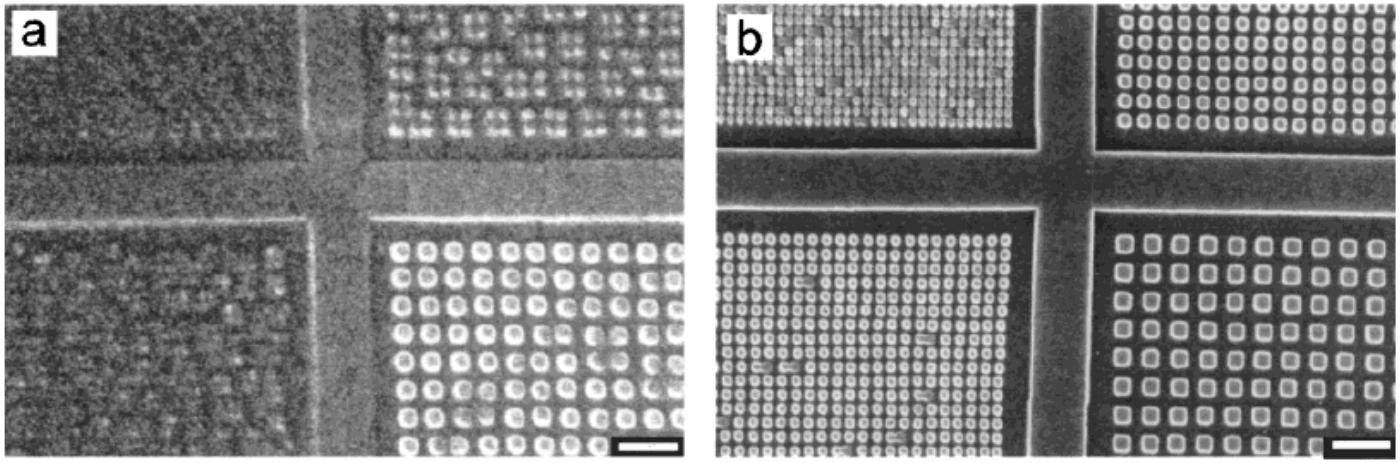

Figure 3. Comparison of high-resolution pattern replication by (a) Sylgard 184 with a compression modulus of 2 N/mm^2 and (b) material B with a compression modulus of 9.7 N/mm^2, bar = 1 μm. Squares of 250 $\times$ 250 nm^2 (lower right quadrant) already appear rounded in the Sylgard 184 stamp and are not stable enough for contact printing. Material B accurately replicates structures down to 80 nm (upper left quadrant). The height of the structures is 100 nm in both cases.

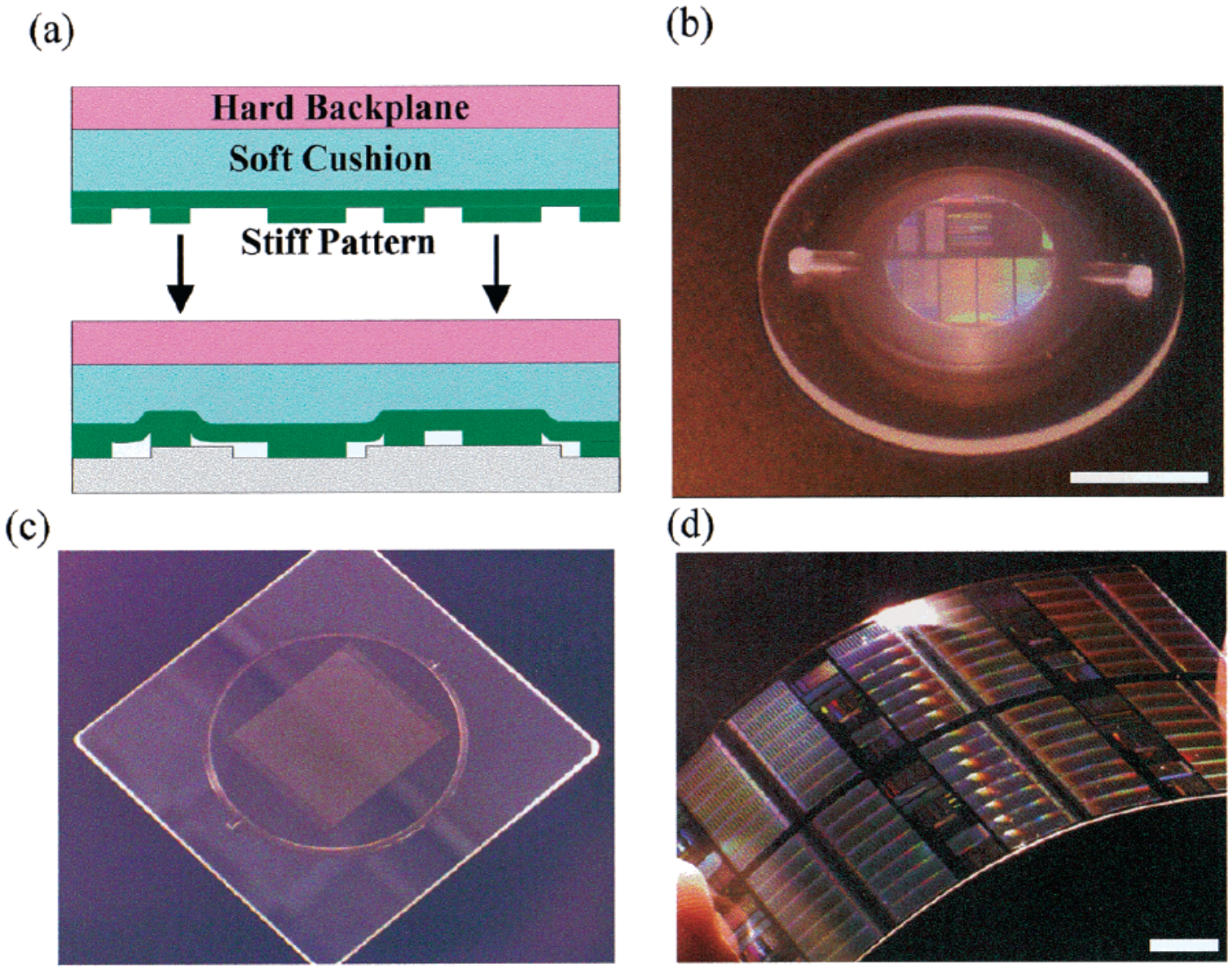

Figure 4. Examples of stamps. (a) Scheme of a trilayer stamp (glass backplane, elastomeric cushion, hard polymer, upper part) and a trilayer stamp in contact with an uneven substrate illustrating improved adaptivity (lower part). (b) Trilayer stamp with 270 nm features, bar = 10 mm. (c) Stamp 1 mm thick having >5 μm patterns molded in a soft siloxane polymer on a 125 mm glass plate. (d) Example of a two-layer thin film stamp composed of a 100 μm glass backplane and a 30 μm thick film of material B with 270 nm features, bar = 10 mm.

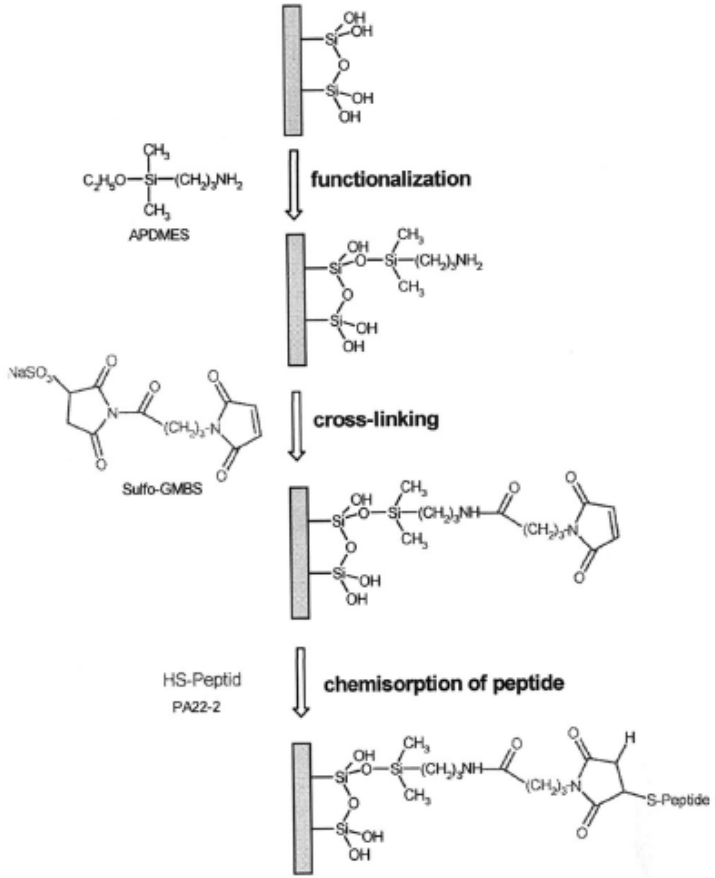

Fig. 1. Covalent attachment of the peptide PA22-2 to silicon oxide surfaces. First silanol groups on the silicon oxide surface are formed by hydroxylation using aqueous sulfuric acid. The ethoxy group of APDMES is hydrolysed by a nucleophilic displacement forming a reactive silanol group which forms a siloxane linkage to the activated surface. Sulfo-GMBS is then used as a heterobifunctional cross linker which is reactive to amino groups at one end and to sulfhydryl groups at the other. In the first step the NHS ester reacts with the amino surface as a nucleophil with release of the sulfo-NHS leaving group forming an amide bond. This allows PA22-2 to react with the sulfhydryl group of its N-terminus forming a thioether bond in a alkylation reaction with the C=C bond of the maleimide ring.

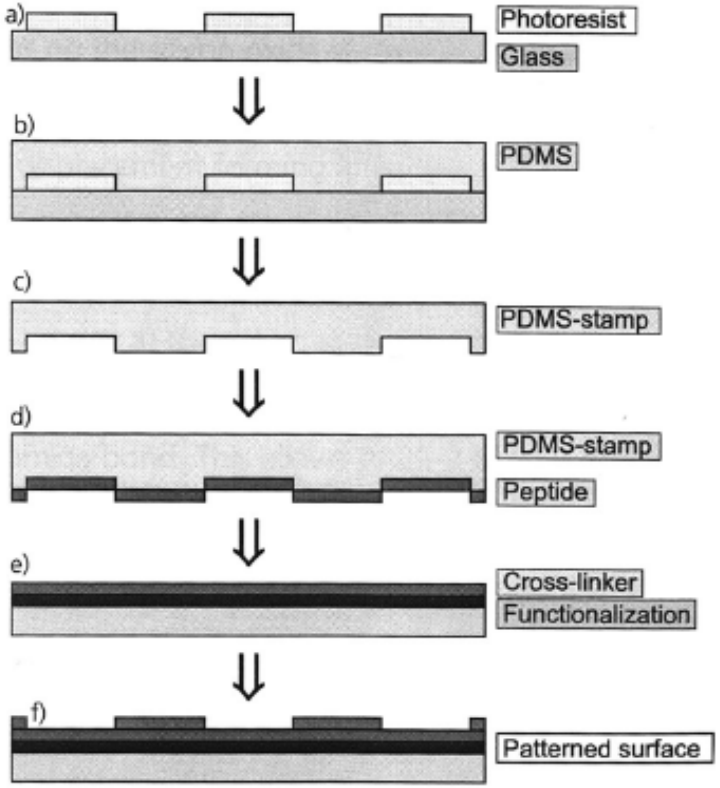

Fig. 2. Steps of stamp production (a–c) and surface modification via μCP (d–f). The masterstamp (a) is covered with the silicone mixture (b). After 4 h of curing at 60°C, the PDMS-stamp is peeled off as a negative cast of the masterstamp (c). After inking the stamp with an aqueous peptide solution (d) it is transferred to the silicon surface pre-treated with aminosilane and cross-linker (e) resulting in a peptide patterned surface (f).

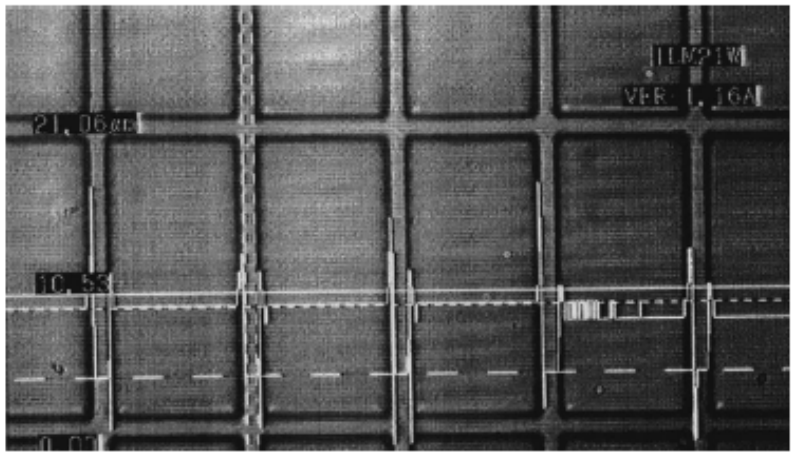

Fig. 3. SEM photograph of a master stamp (defined as 3 μm stamp) including the height profile. The glass surface forms the bottom of the mould for the later lines of the stamp structure. To form the grid-structure of the mould a photoresist is spin-coated, irradiated and developed. The not-removed photoresist with a thickness of 4.5 μm built the area in-between the lines. The line width at the bottom of the mould is determined to 3.4 μm.

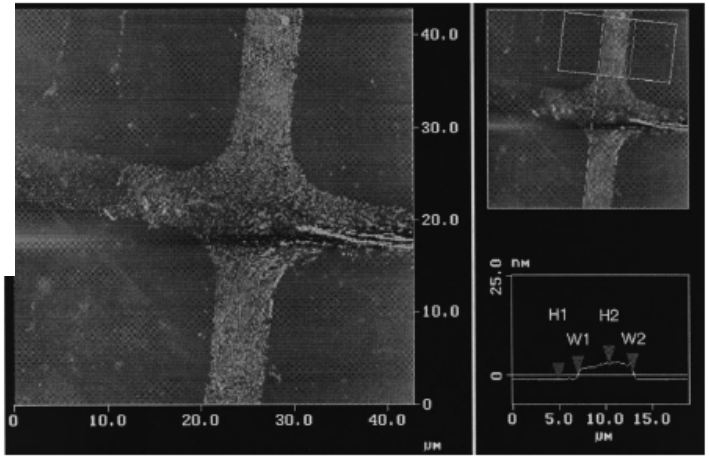

Fig. 4. AFM image of a peptide imprint. The size of the scanned area is 42.8 × 42.8 μm. Height (H1, H2) and slope of the flanks (at W1, W2) of the imprint are evaluated from the profile plot averaged over an area indicated in the inset.

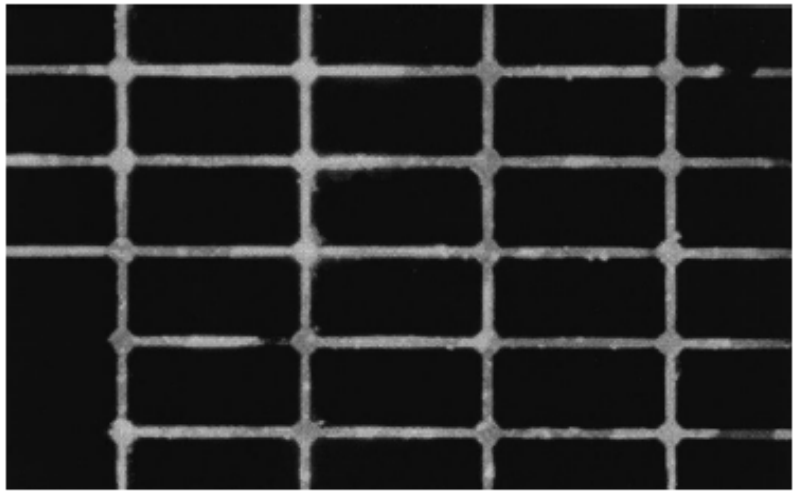

Fig. 5. Fluorescence image of an imprint of fluorescein-labeled PA22-2. The pattern consists of 5 μm wide lines crossing in 50 respective 100 μm. The crossing points consist of square-shaped nodes, 12 μm in diameter.

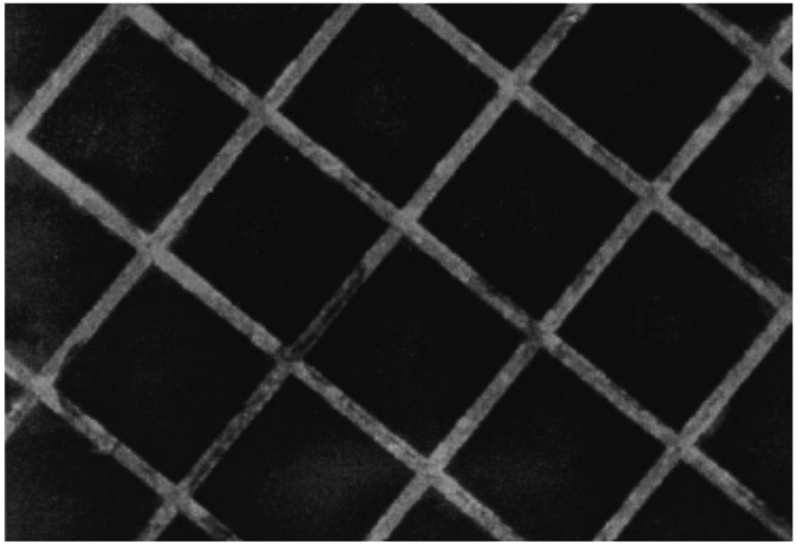

Fig. 6. Immunostaining for the cell-active sequence IKVAV of PA22-2 with a polyclonal rabbit antiserum and a fluorescein-labeled secondary antibody. The grid pattern consists of 5 μm wide lines crossing in 50 μm.

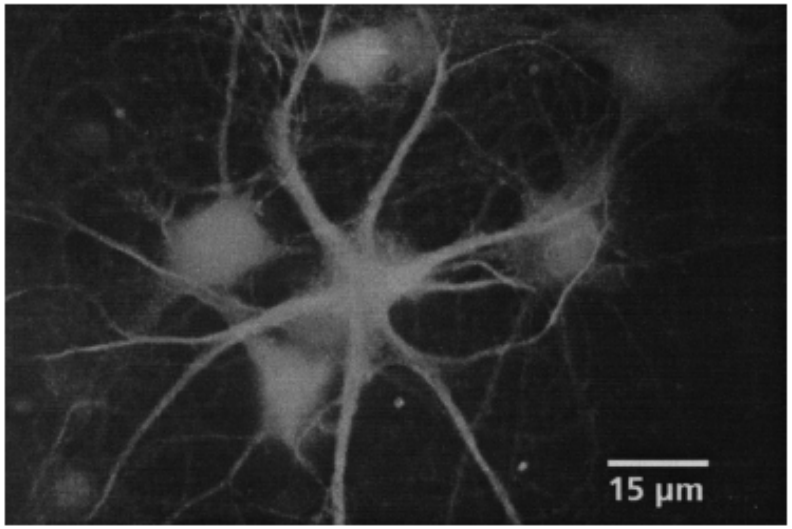

Fig. 7. Hippocampal neurones in a serum-containing medium after 6 days in culture (DIV). The photograph shows a texas-red-staining with the glia-specific marker GFAP and a FITC-staining with neuron-specific marker for NMDAR1 (*N*-methyl-D-aspartate). The glial cell in the centre is surrounded by five neurones. In a later stage of culturing, a confluent layer of glial cells with neurones growing on top of this layer will be formed.

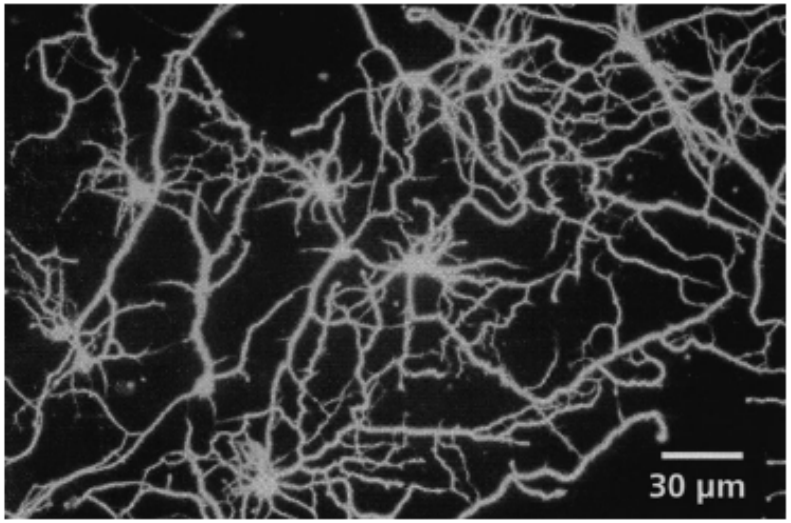

Fig. 8. Hippocampal neurones on a silicon oxide surface uniformly activate with peptide PA22-2 after 5 DIV. Immunostaining with Cy3 for tau proteins shows a uniform distribution over cell somata and neurites.

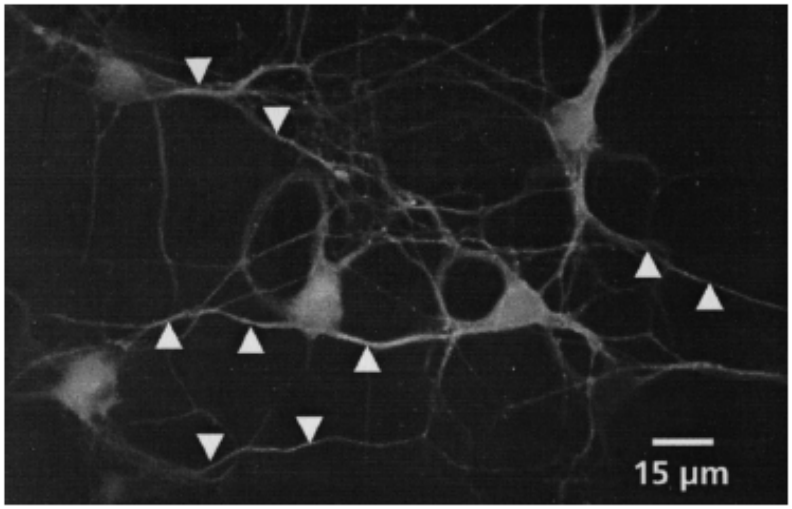

Fig. 9. Acquisition of neuronal polarity in a network of hippocampal neurones after 6 DIV under serum-free conditions. The surface was uniformly functionalised with peptide PA22-2. The photograph shows a polar network of five neurones stained with FITC for the axon-specific marker GAP43 ($\wedge$) and with texas red for the dendrite-specific marker MAP2 ($\vee$).

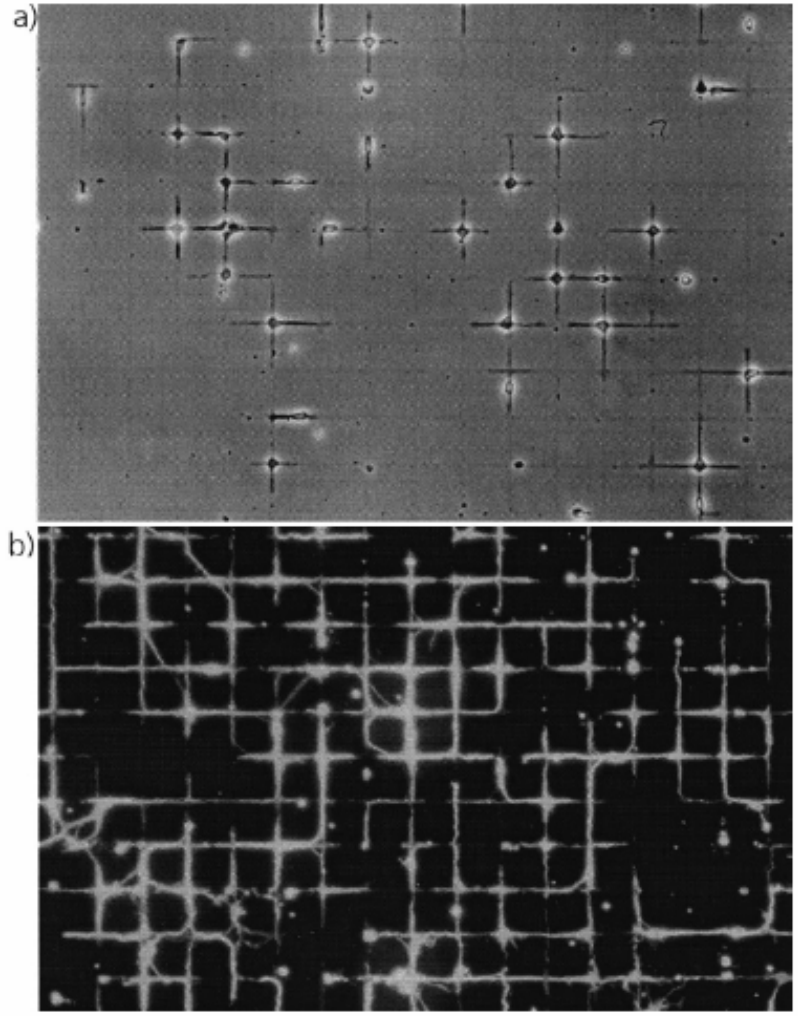

Fig. 10. Response of hippocampal neurones to a grid pattern of PA22-2. (a) Phase-contrast image of neurones after 1 day of culture on 5 µm wide lines of PA22-2 crossing in 50 µm. (b) Immunocytochemical staining with a fluorescein-labeled antibody for tau protein after 3 days in culture on a similar peptide pattern.

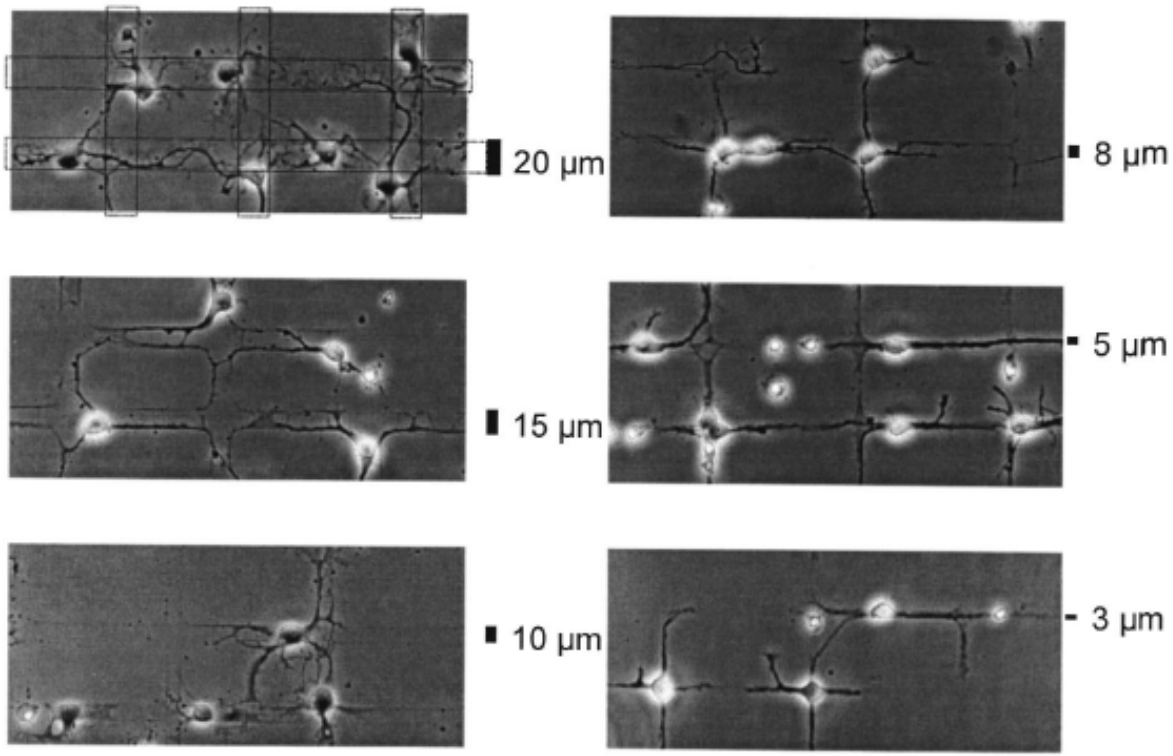

Fig. 11. Hippocampal neurones on grid patterns of PA22-2 in different dimensions after 3 days in culture. The images show the influence of decreasing line widths from 20 down to 3 µm on the morphology of the resulting neuronal networks. In case of the rather narrow lines of the peptide PA22-2 pattern (8, 5, 3 µm), cell bodies preferentially occupy the crossing points of the grid. For broader tracks (20, 15, 10 µm), the location of the cell bodies on the peptide lines is not clearly defined and the outgrowing neurites change their direction many times.

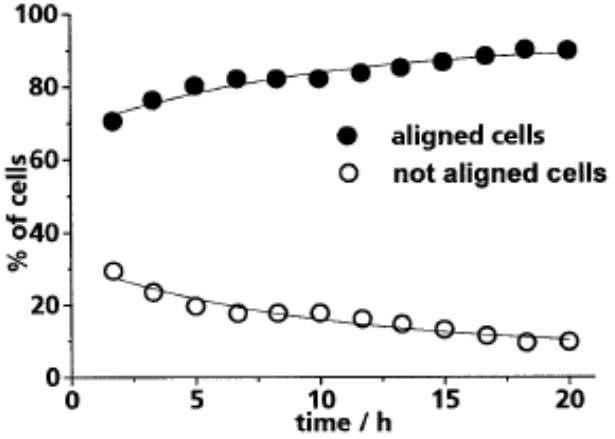

Fig. 12. Cell compliance on grid pattern (5 μm lines crossing in 50 μm) of peptide. The graph shows that even after 2 h in culture, 70% of the cells are aligned. This number increases up to 90% within the first 20 h in culture.

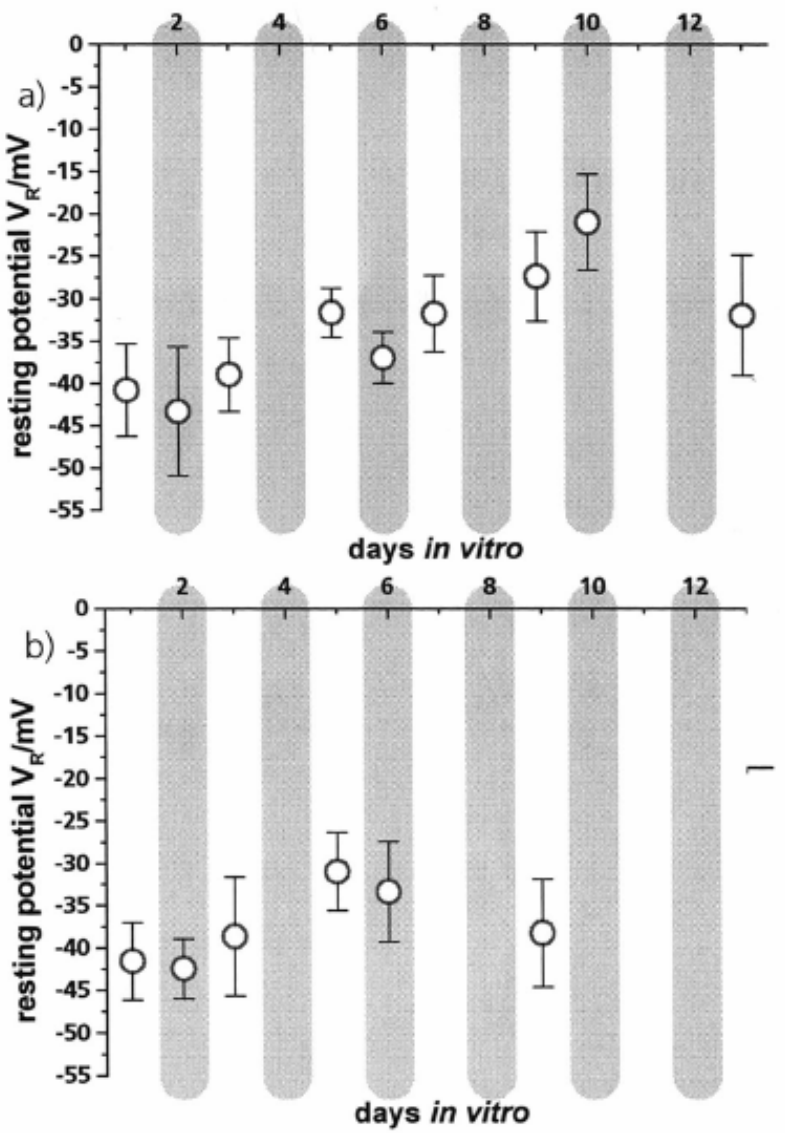

Fig. 13. Development of resting membrane potential for (a) unpatterned and (b) patterned neurones with time in culture on 5 μm peptide lines of a grid pattern. Patterned and unpatterned cells show a comparable development of their resting potentials. Already after 1 day in culture, single neurones could electrically be stimulated to action potentials.

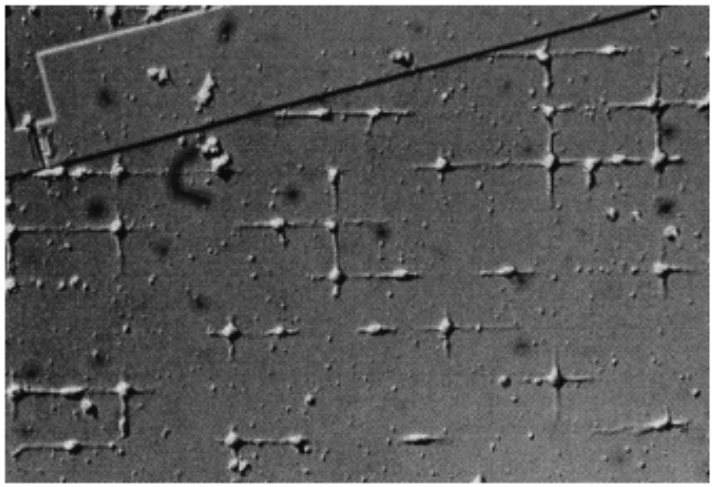

Fig. 14. Neuronal network of hippocampal neurones on a FET-chip after 2 days in culture. The cellular network reflects the geometry of the underlying peptide pattern (5 μm lines crossing in 50, respectively 100 μm).

Fabricating Microarrays of Functional Proteins Using Affinity Contact Printing**

Angew. Chem. Int. Ed. **2002**, *41*, No. 13

Jean Philippe Renault, André Bernard, David Juncker, Bruno Michel, Hans Rudolf Bosshard, and Emmanuel Delamarche*

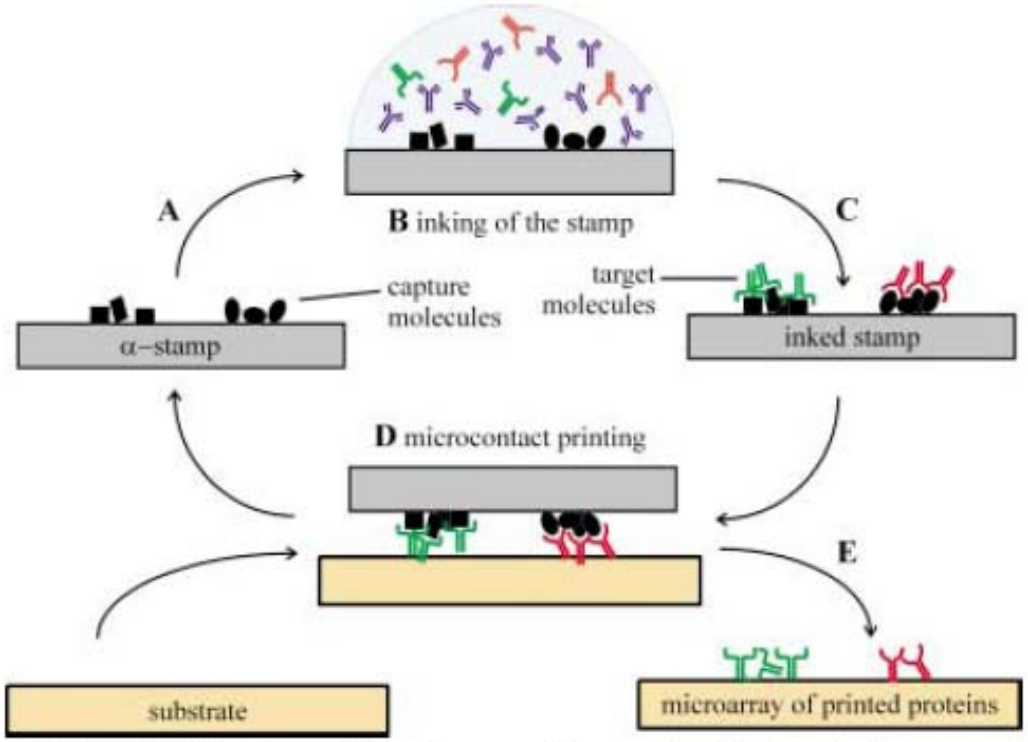

Figure 1. Microarrays of proteins on surfaces can be fabricated using an α-stamp derivatized with various capture sites that can extract target biomolecules from a complex solution and release them on a surface in a single microcontact-printing step. The α-stamp can be reused for several inking and printing cycles.

a) Fabricating the μ-wells and activating the PDMS stamp

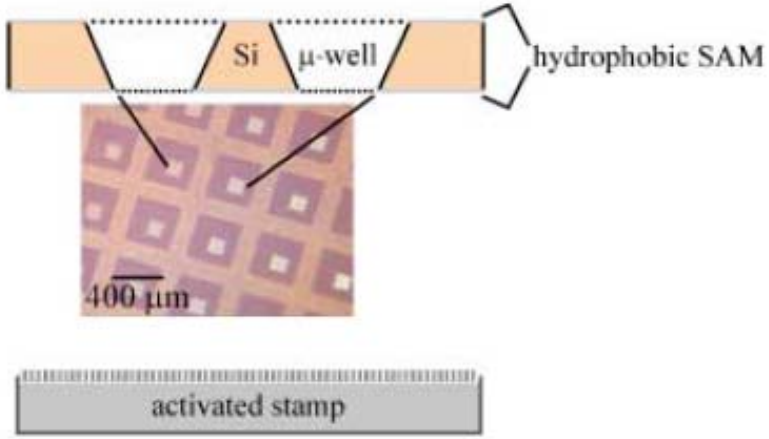

b) Placing the μ-wells and filling them with solutions of antigens

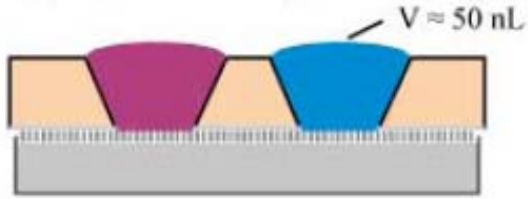

c) Removing the μ-wells under a buffer and rinsing the stamps

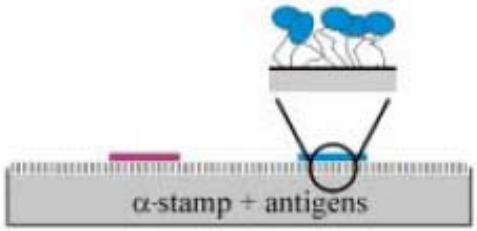

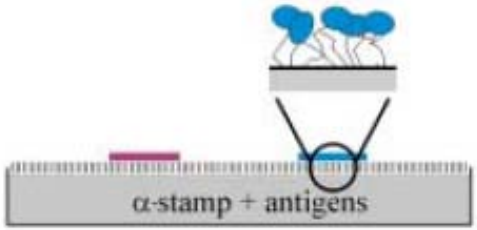

d) Inking the stamp with a solution of target antibodies and printing the captured antibodies

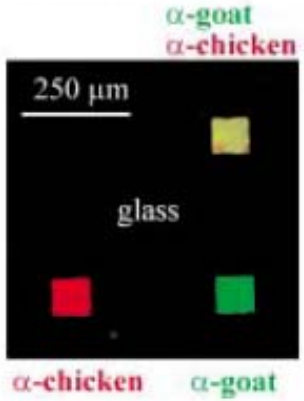

Figure 2. Preparation of a microarray of proteins using an α-stamp patterned with microwells. a) The microwells are formed in a Si wafer, and the PDMS stamp is derivatized with cross-linkers for proteins. b) The contact of the microwells with the activated stamp localizes the attachment of capture molecules from solution to the area of the stamp exposed in each microwell. c) After separating it from the microwells, rinsing and drying, the α-stamp is ready for use. d) The α-stamp in this example had an empty capture site and sites with covalently attached anti-chicken antigens, anti-goat antigens, and protein A. Inking the α-stamp consists of the binding of antibodies (here tagged fluorescently) from solution to their specific antigens on the surface of the stamp. After rinsing and drying the inked α-stamp, the antibodies can be printed onto a glass surface and visualized by fluorescence microscopy.

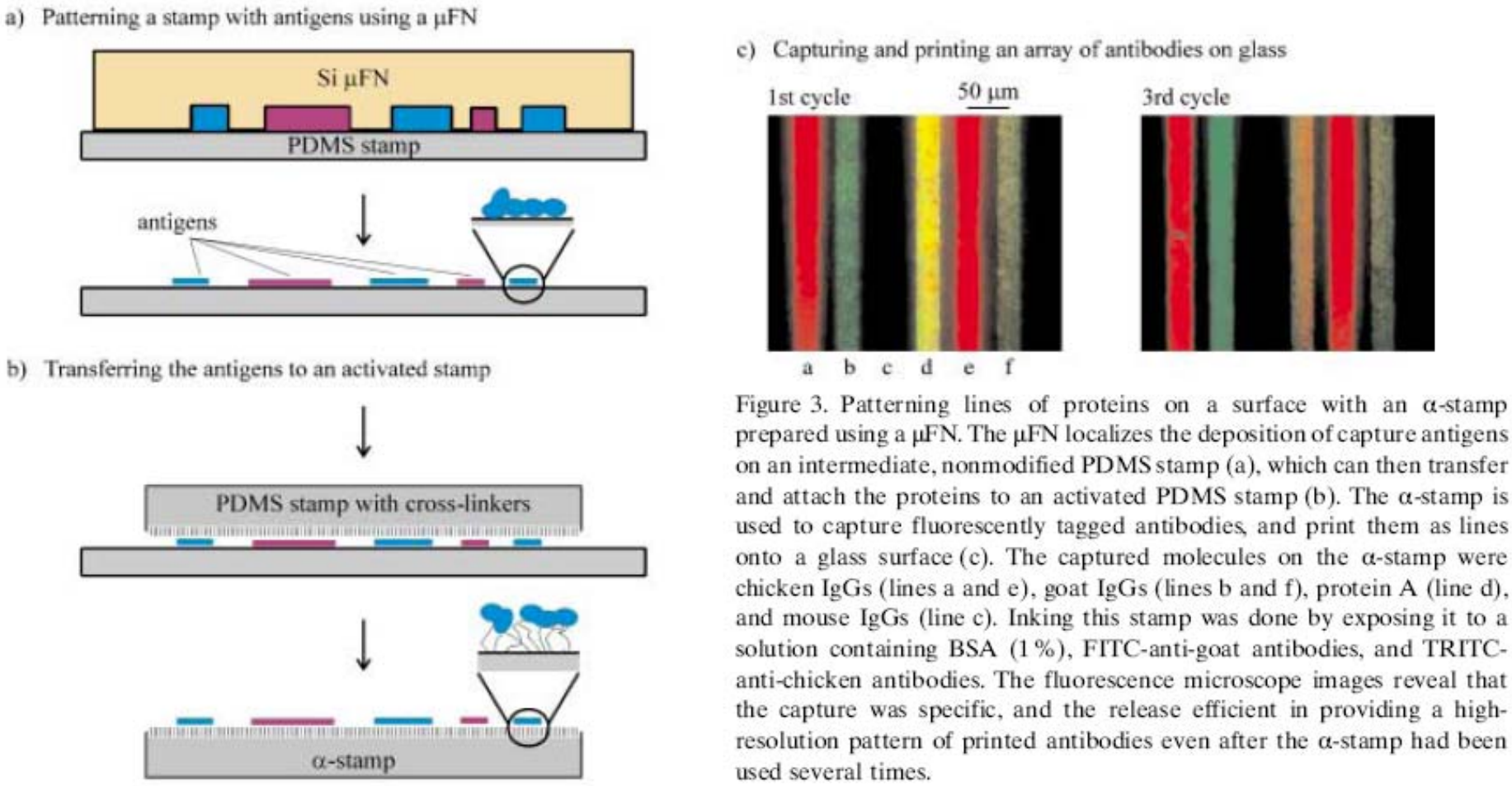

Figure 3. Patterning lines of proteins on a surface with an α-stamp prepared using a μFN. The μFN localizes the deposition of capture antigens on an intermediate, nonmodified PDMS stamp (a), which can then transfer and attach the proteins to an activated PDMS stamp (b). The α-stamp is used to capture fluorescently tagged antibodies, and print them as lines onto a glass surface (c). The captured molecules on the α-stamp were chicken IgGs (lines a and e), goat IgGs (lines b and f), protein A (line d), and mouse IgGs (line c). Inking this stamp was done by exposing it to a solution containing BSA (1 %), FITC-anti-goat antibodies, and TRITC-anti-chicken antibodies. The fluorescence microscope images reveal that the capture was specific, and the release efficient in providing a high-resolution pattern of printed antibodies even after the α-stamp had been used several times.

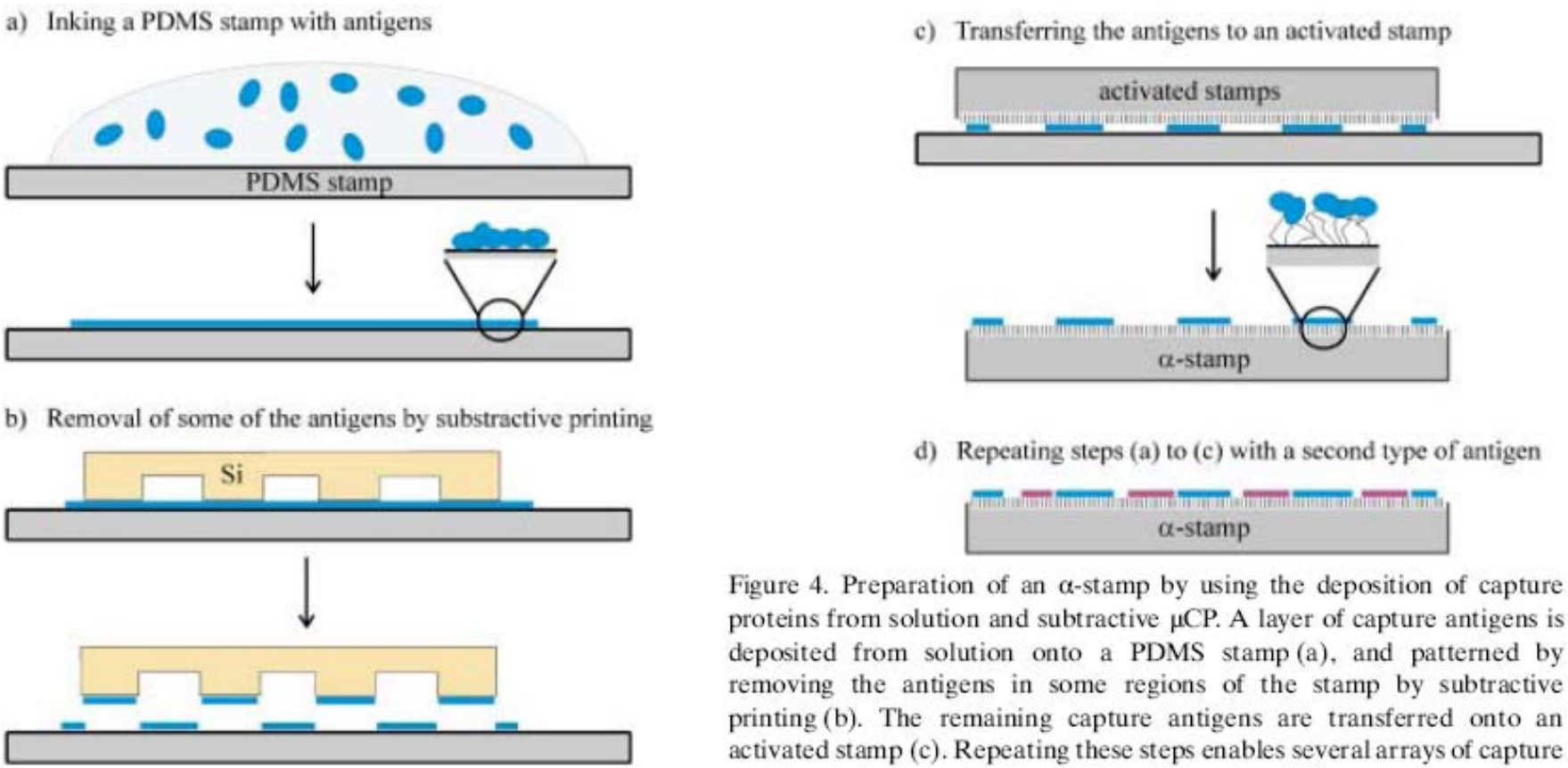

Figure 4. Preparation of an α-stamp by using the deposition of capture proteins from solution and subtractive μCP. A layer of capture antigens is deposited from solution onto a PDMS stamp (a), and patterned by removing the antigens in some regions of the stamp by subtractive printing (b). The remaining capture antigens are transferred onto an activated stamp (c). Repeating these steps enables several arrays of capture proteins to be successively added to the α-stamp (d).

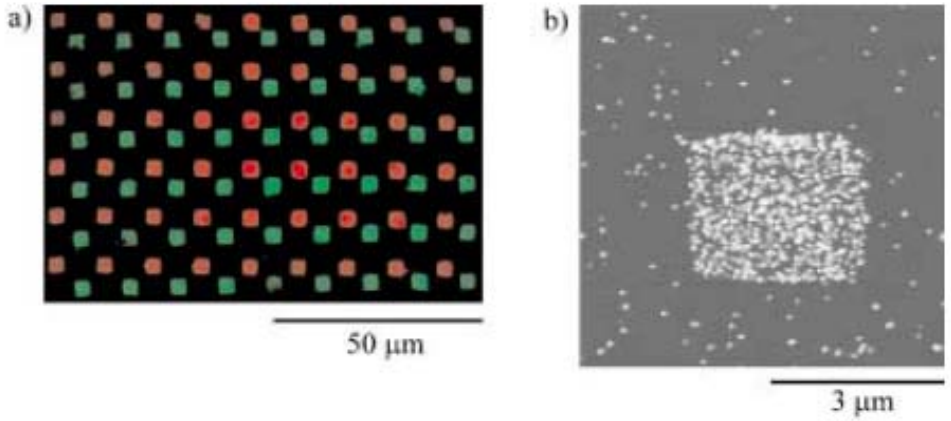

Figure 5. Arrays of anti-chicken antibodies and anti-goat antibodies printed using an αCP having 10^4 equivalent capture sites per mm^2 that consist of immobilized chicken and goat antigens. a) Fluorescence microscope image showing the placement of the TRITC-anti-chicken and FITC-anti-goat antibodies from a stamp onto a glass substrate. b) AFM image obtained on a spot of the array in which the printed anti-goat antibodies bound to Au-labeled goat antigens presented in solution. Detection of this binding was done by staining the Au labels with electroless-deposited silver particles of an average diameter of 80 nm.

For a cell to move, it must adhere to a substrate and exert traction. Adhesion occurs at specific foci at which the actin cytoskeleton on the inside of the cell is linked via transmembrane receptors (integrins) to the extracellular matrix on the outside. These adhesion sites are composed of complexes of more than 50 different proteins

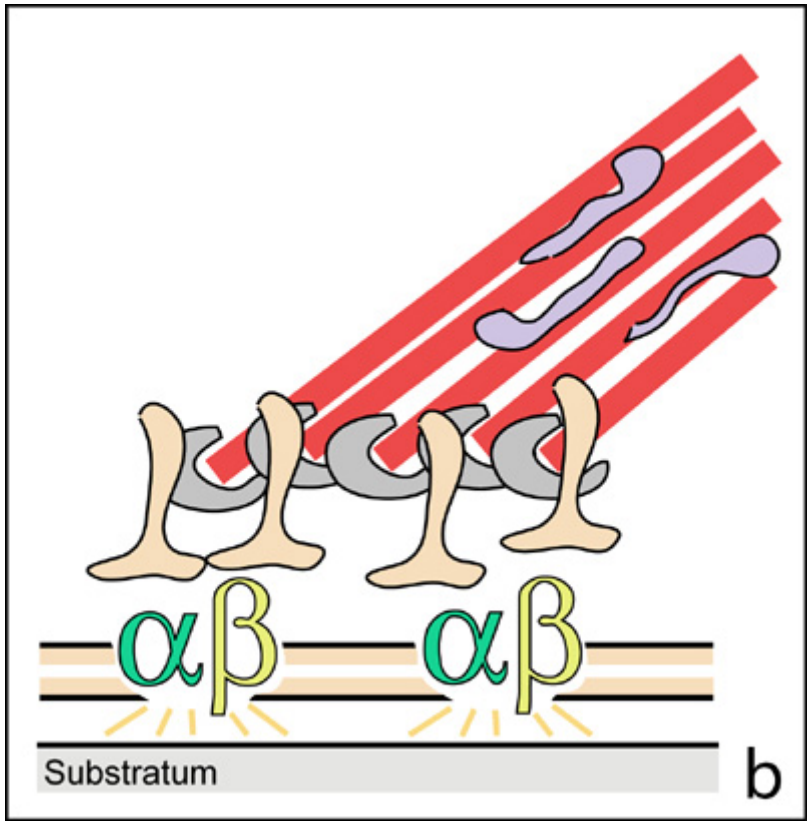

Highly simplified schematic illustration of the organisation of a focal adhesion. Transmembrane integrins (alpha/beta) bind to matrix ligands on the outside of the cell, and to a complex of molecules inside the cell that link to actin filaments. At focal adhesions, the actin filaments are bundled by actin filament cross-linkers, including the contractile protein myosin. Tension in the bundle, generated by myosin, is required to maintain the clustering of integrins and the integrity of focal adhesions

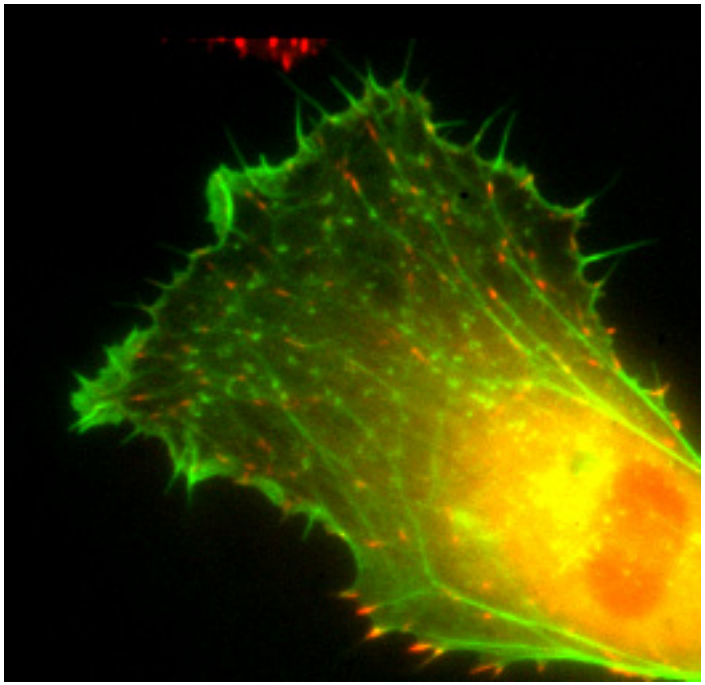

The formation of substrate adhesion sites in a migrating goldfish fibroblast. The cell was transfected with GFP-actin (green) and microinjected with rhodamine-tagged vinculin (an adhesion component; red). The protruding cell front is marked by a diffuse band of actin filaments (the lamellipodium), which contains radial filament bundles (filopodia) that project beyond the cell edge. Different types of adhesion foci (red) can be distiguished: small foci in association with lamellipodia and filopodia (focal complexes) and, behind the lamellipodium, larger foci associated with actin filament bundles (focal adhesions). Focal adhesions are also observed at the periphery of retracting cell edges (bottom region of figure). Focal complexes and focal adhesions in the advancing front remain stationary, relative to the substrate, whereas, focal adhesions at the retracting edges can slide.

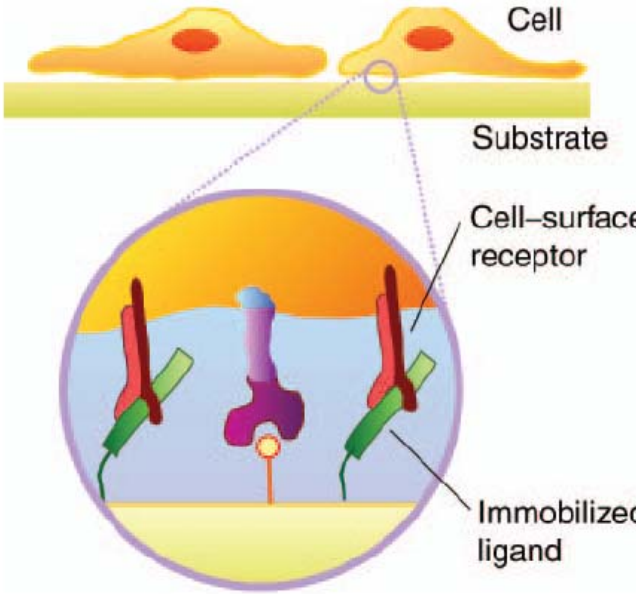

Figure 1. Most cells are adherent and must attach and spread on a matrix. The interaction of a cell with the substrate relies on the binding of cell–surface receptors with ligand proteins that are adsorbed to the material.

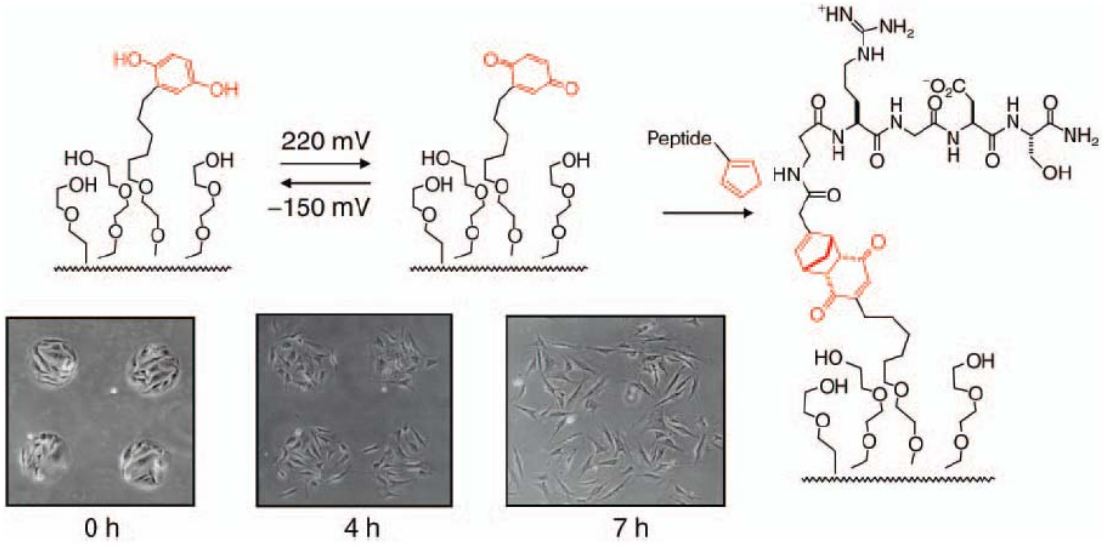

Figure 3. Design of a substrate that electrically turns on the immobilization of a ligand. An electrical potential converts a hydroquinone group to benzoquinone, which serves to immobilize a peptide ligand. The dynamic surfaces can initiate the migration of cells that are originally confined to 200 μm circular regions on the substrate.

Using electroactive substrates to pattern the attachment of two different cell populations

5992–5996 | PNAS | May 22, 2001 | vol. 98 | no. 11

Muhammad N. Yousaf, Benjamin T. Houseman, and Milan Mrksich*

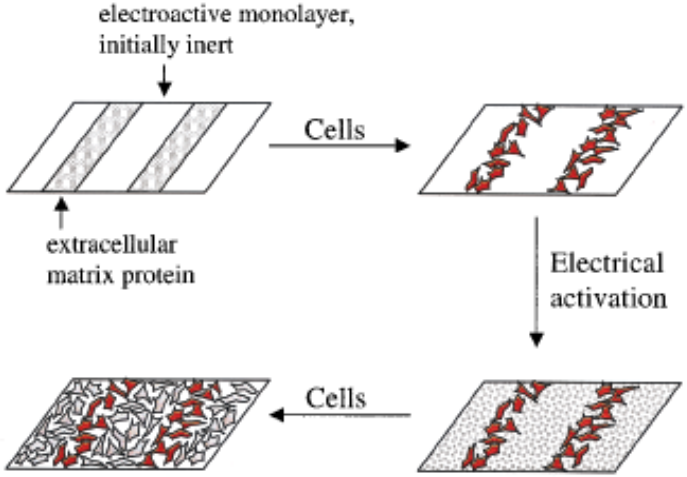

Fig. 1. Strategy for patterning two different cell types to a substrate. The method starts with a surface that is patterned into regions that promote cell attachment (i.e., regions coated with extracellular matrix proteins) and regions that are inert to cell attachment, but that can be converted to promote attachment by the application of an electrical potential. After cells attach to the first set of regions, the inert set of regions can be activated electrically so that a second cell population can attach, generating a patterned coculture.

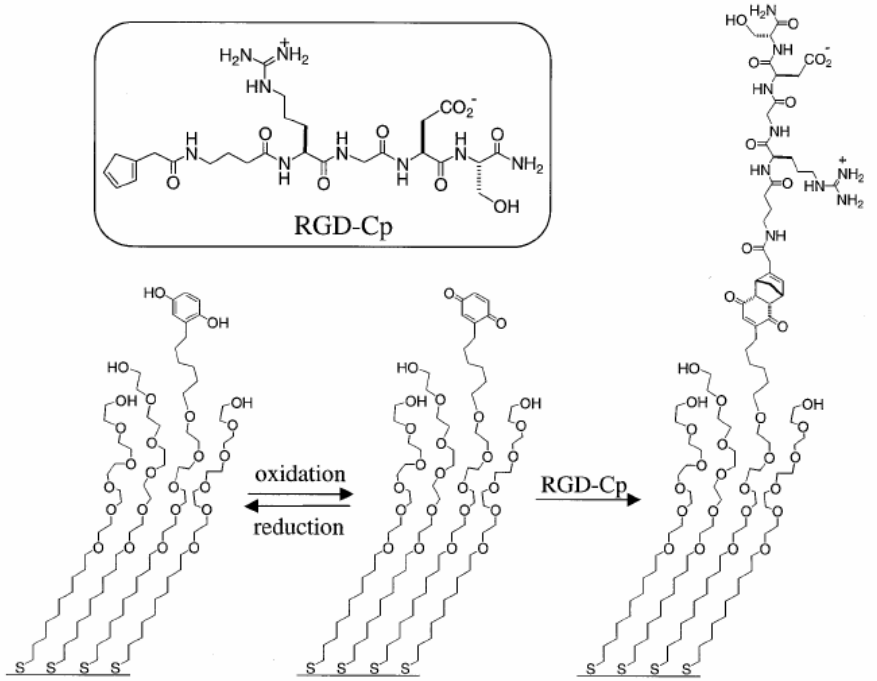

Fig. 2. Molecular strategy for creating substrates that can be electrically switched to permit cell attachment. A monolayer presenting a mixture of hydroquinone groups and penta(ethylene glycol) groups (*Left*) is converted to a monolayer presenting the corresponding quinone groups (*Center*) by application of a potential to the underlying gold (500 mV versus Ag/AgCl). Both monolayers are inert to the attachment of cells. Addition of a conjugate of cyclopentadiene and the peptide Gly-Arg-Gly-Asp-Ser-NH_2 (RGD-Cp) to the monolayer presenting the quinone group results in the Diels-Alder-mediated immobilization of peptide (*Right*). 3T3 fibroblasts attach and spread on the resulting surface. Monolayers presenting the hydroquinone group are unaffected by the treatment with RGD-Cp and remain inert to cell attachment.

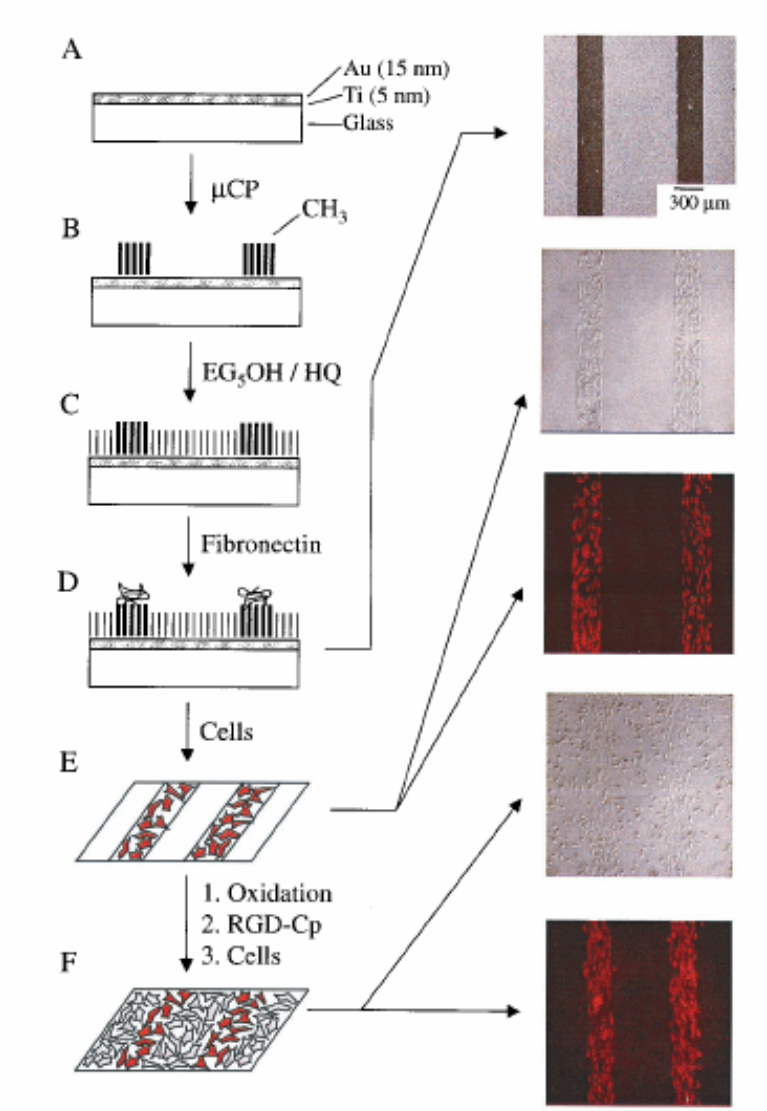

Fig. 3. Use of an electroactive substrate to pattern two cell populations into a coculture. (*A*) Substrates were prepared by evaporating titanium (5 nm) and then gold (15 nm) onto glass coverslips. (*B*) Microcontact printing was used to pattern hexadecanethiolate into lines that are 300 μm wide and separated by 800 μm. (*C*) A second monolayer was assembled on the remaining regions of gold by immersing the substrate into a solution of hydroquinone-terminated alkanethiol (HQ) and penta(ethylene glycol)-terminated alkanethiol (EG_5OH). (*D*) The substrate then was immersed in a solution of fibronectin in PBS for 4 h. A scanning electron micrograph shows that protein adsorbed only to the methyl-terminated regions of the monolayer. (*E*) 3T3 fibroblasts attached only to the regions presenting fibronectin, and when cultured in serum-containing media, divided to fill these regions entirely. The surrounding inert monolayer strictly confined the cell to the rectangular regions. (*F*) Electrochemical oxidation of the monolayer in the presence of media containing RGD-Cp (2 nM) led to the immobilization of the peptide. Fluorescence microscopy shows that the two cell populations are patterned on the substrate. All micrographs were taken by ×5 magnification.

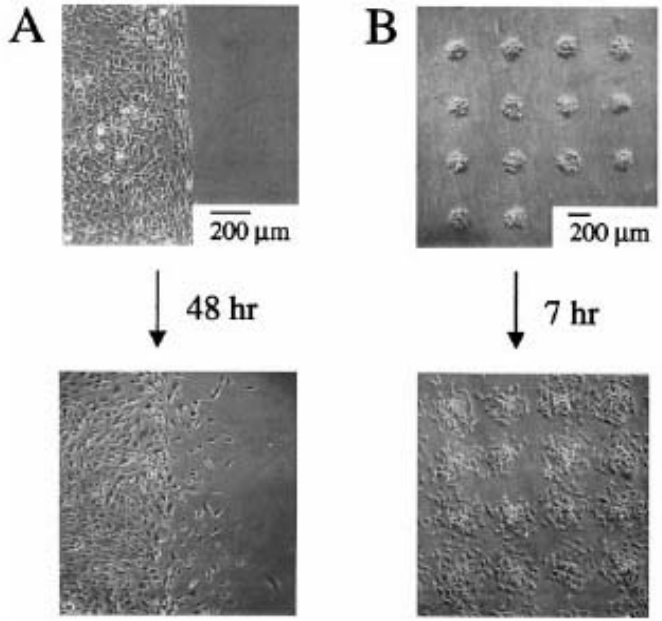

Fig. 4. The onset of migration into the second set of regions after electrochemical activation and peptide immobilization depends on the geometric features of the pattern. Cells patterned along a straight edge (*A*) showed little migration after 48 h, whereas cells patterned to 200-μm circles showed extensive migration after only 7 h (*B*). All micrographs were taken at ×5 magnification.

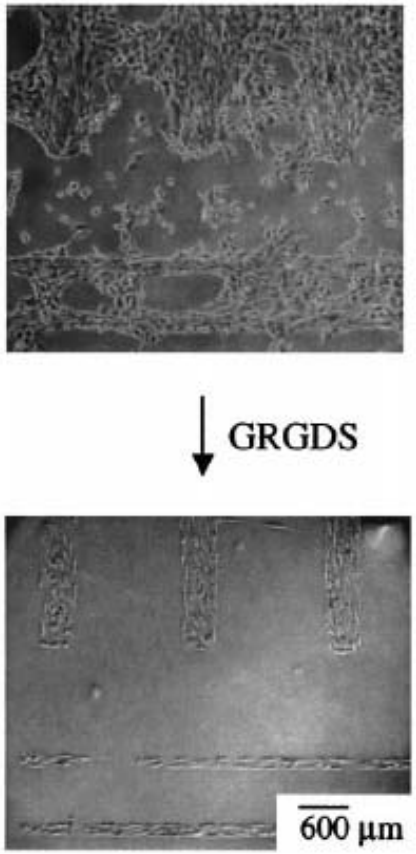

Fig. 5. Selective detachment of cells adhered to regions of the substrate presenting the RGD peptide among penta(ethyene glycol) groups. A patterned coculture was prepared as described in Fig. 3 *Left*. Addition of soluble peptide (GRGDS, 2 mM for 1 h) resulted in the detachment of cells only from the regions of the monolayer presenting peptide conjugates, indicating the specificity of the cell-substrate interaction. Micrographs were taken at ×5 magnification.

Light-Driven Motion of Liquids on a Photoresponsive Surface

Kunihiro Ichimura,* Sang-Keun Oh, Masaru Nakagawa

2 JUNE 2000 VOL 288 SCIENCE

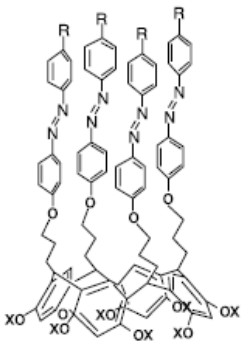

Fig. 1. Macrocyclic amphiphile tethering photochromic azobenzene units (CRA-CM).

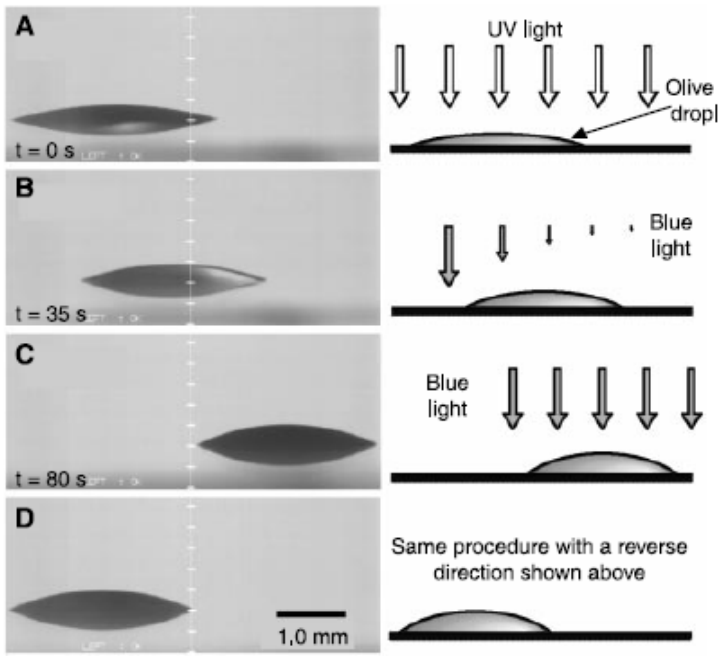

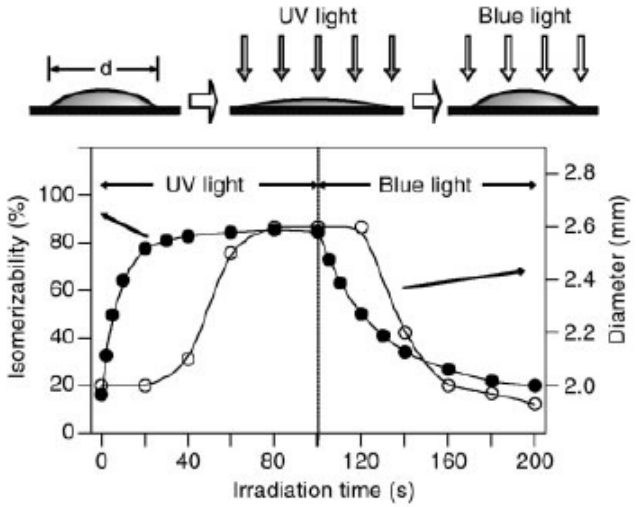

Fig. 2 (left). Lateral photographs of light-driven motion of an olive oil droplet on a silica plate modified with CRA-CM. The olive oil droplet on a cis-rich surface moved in a direction of higher surface energy by asymmetrical irradiation with 436-nm light perpendicular to the surface. (**A** to **C**) The sessile contact angles were changed from 18° (A) to 25° (C). (**D**) The moving direction of the droplet was controllable by varying the direction of the photoirradiation. **Fig. 3 (right).** Correlation between the level of cis isomer (solid circles) and the diameter (open circles) of an NPC-02 droplet placed on a silica plate modified with CRA-CM upon homogeneous irradiation with UV and blue light (1.0 mW cm^{-2}). The level of photoisomerization was estimated by monitoring the UV-visible absorption spectrum of the plate. The viscosity of NPC-02 is 9.8 mPa s at 23°C. The sessile contact angles before and after UV irradiation were 24° and 11°, respectively.

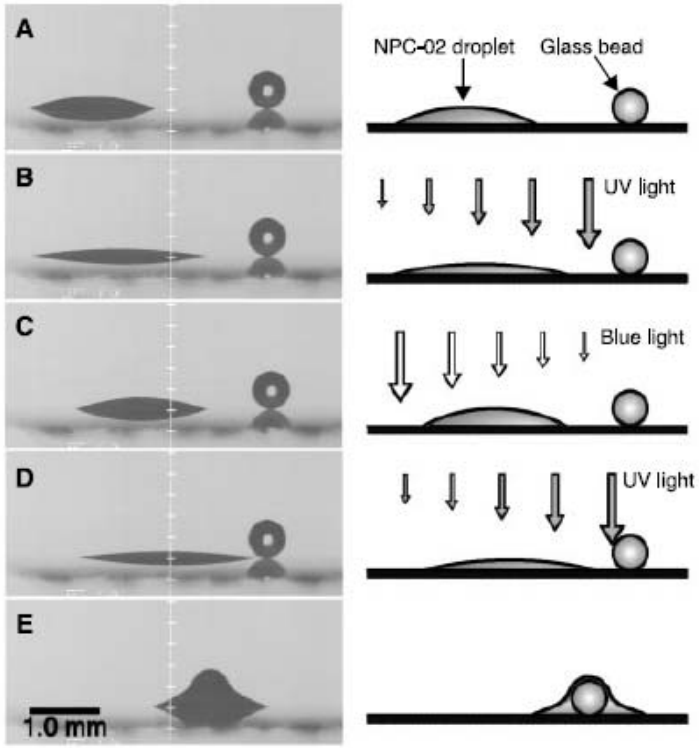

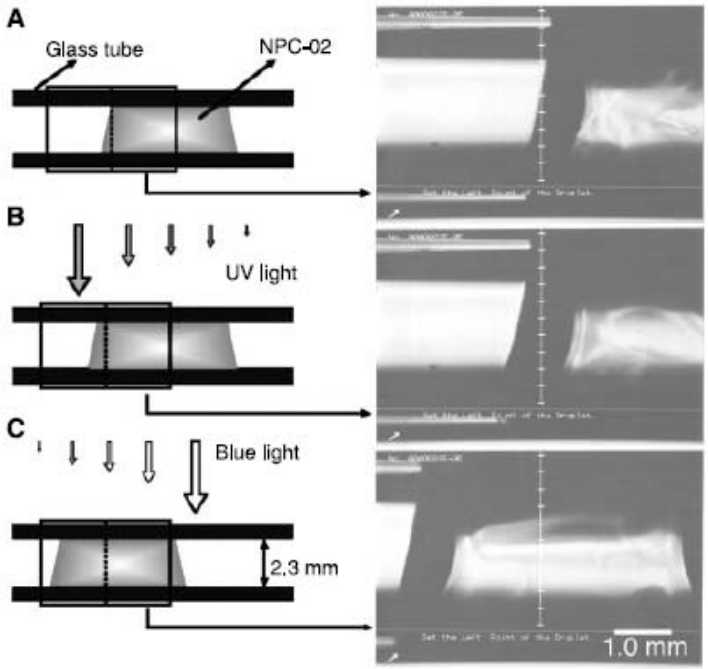

Fig. 5 (left). Light-driven motion of an NPC-02 droplet on a CRA-CM–modified plate to capture a glass bead (diameter ~0.5 mm). A droplet was placed on a CRA-CM–modified plate (**A**), followed by UV light irradiation at the right edge of the droplet to cause an asymmetrical spreading (**B**). Subsequent irradiation with blue light at the left edge resulted in dewetting, leading to the displacement of the droplet (**C**). The repetition of this stepwise photoirradiation resulted in the approach of the droplet to the bead (**D**), which was finally captured by the liquid (**E**). **Fig. 6 (right).** Light-driven displacement of an NPC-02 droplet in a glass tube. A droplet of NPC-02 was placed in the tube (**A**), and one edge of the droplet was exposed to UV light, leading to the slight advancement of the droplet (**B**). Subsequent irradiation with blue light at the opposite edge pushed the droplet to the left (**C**).

Fabrication of reconfigurable protein matrices by cracking

Mechanically Controlled Switching

XIAOYUE ZHU[1], KRISTEN L. MILLS[2], PORTIA R. PETERS[2], JOONG HWAN BAHNG[1], ELIZABETH HO LIU[1], JEONGSUP SHIM[1], KEIJI NARUSE[3], MARIE E. CSETE[4], M. D. THOULESS[2,5] AND SHUICHI TAKAYAMA[1,6]*

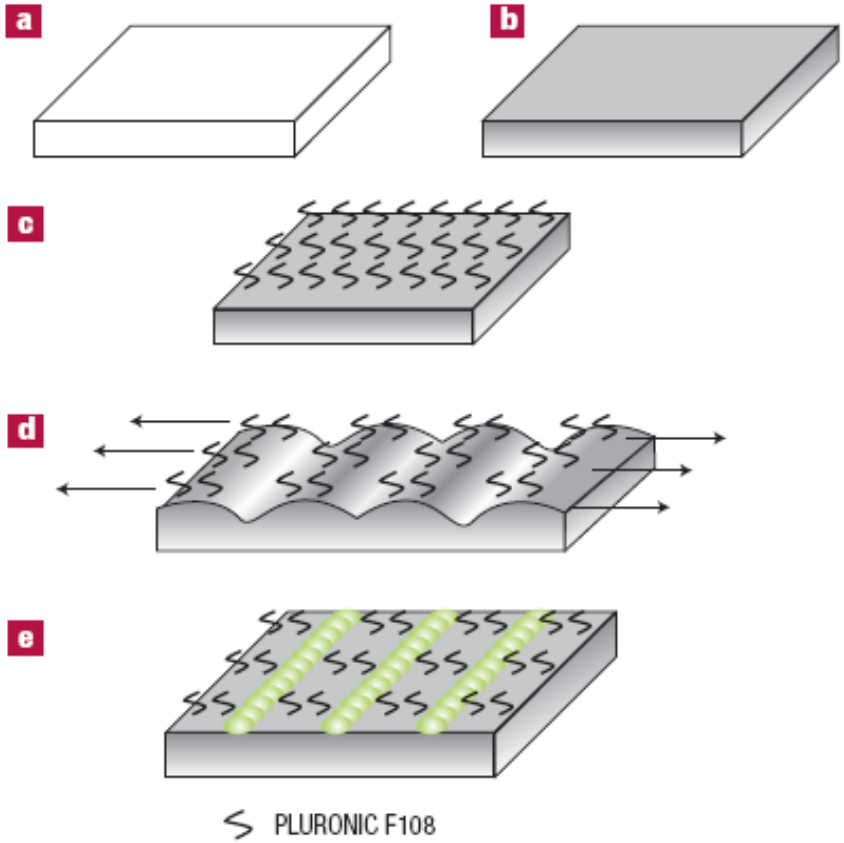

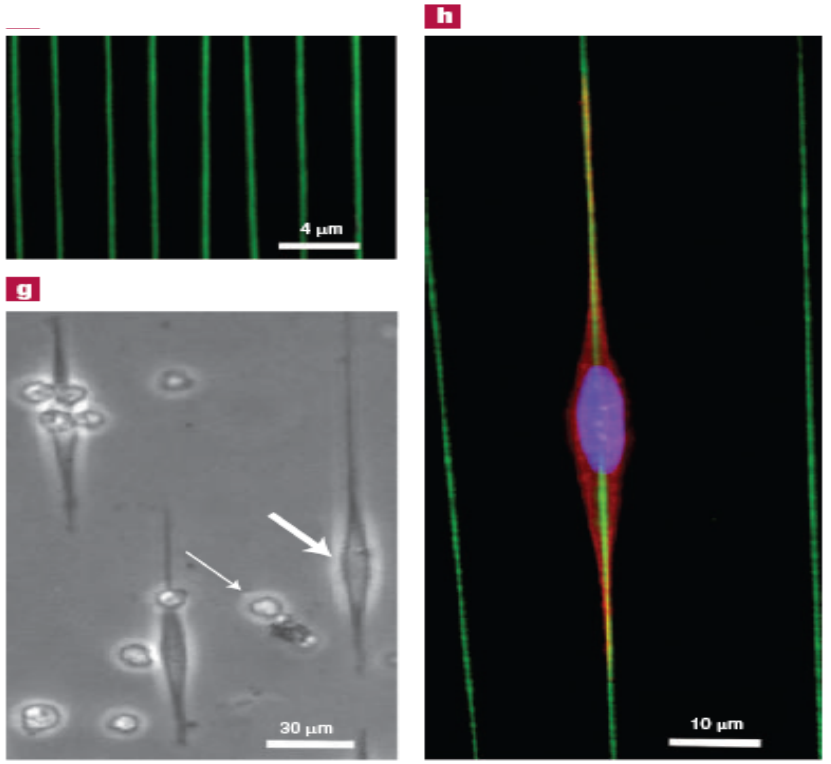

Figure 1 Schematic illustration of crack patterning. a–c, A PDMS slab (**a**) is oxidized (**b**) to generate a brittle surface layer, and coated with Pluronic F108 (**c**), to render the surface resistant to protein adsorption. **d**,**e**, Uniaxial strain is applied to crack the brittle surface layer and expose underlying material that is not resistant to protein adsorption (**d**), onto which proteins can deposit (**e**). **f**, Parallel cracks formed by the procedure using fluorescent protein (FITC-BSA). The image is the substrate in its relaxed state. **g**, A micrograph of C2C12 myoblasts spread on wide cracks and elongated along DQ collagen-coated cracks (thick arrow)—a patented fluorescein-conjugated collagen from Molecular Probes. Cells remain round when not attached to protein-coated cracks (thin arrow). **h**, A C2C12 myoblast cell stained with Phalloidin-TRITC for actin (red), Hoechst 33342 for the nucleus (blue). The cell is attached to a crack coated with DQ collagen (green). After cells were fixed, the substrate was relaxed for imaging.

nature materials | VOL 4 | MAY 2005 | www.nature.com/naturematerials

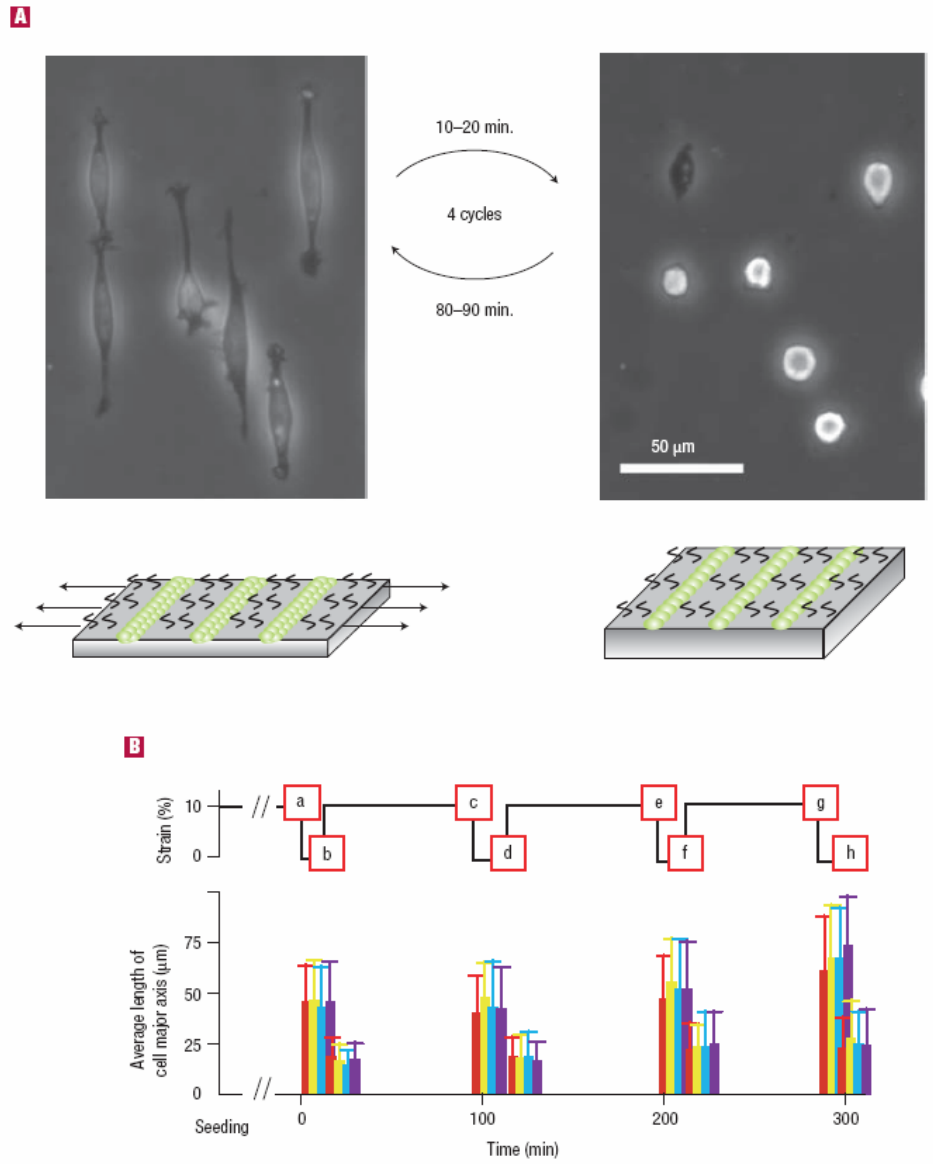

Figure 3 Cyclic switching of cells between modes of spreading and retraction. A, Micrographs of reversible spreading and retraction of C2C12 myoblasts on fibronectin coated cracks. **B**, Average length of the major axis of cells measured for the same group of cells over four cycles of stretching and relaxing (10% strain for ~80 minutes followed by 0% strain for ~20 minutes) applied over a 6-hour period. Cells were analysed in the same four areas, represented by red, yellow, green and purple columns respectively over the four cycles of stretching and relaxing. Error bars are the standard deviation of cell length. See Supplementary Information Fig. S4 for micrographs taken at times corresponding to **a–h**.

Electrically Driven Conformational Switching

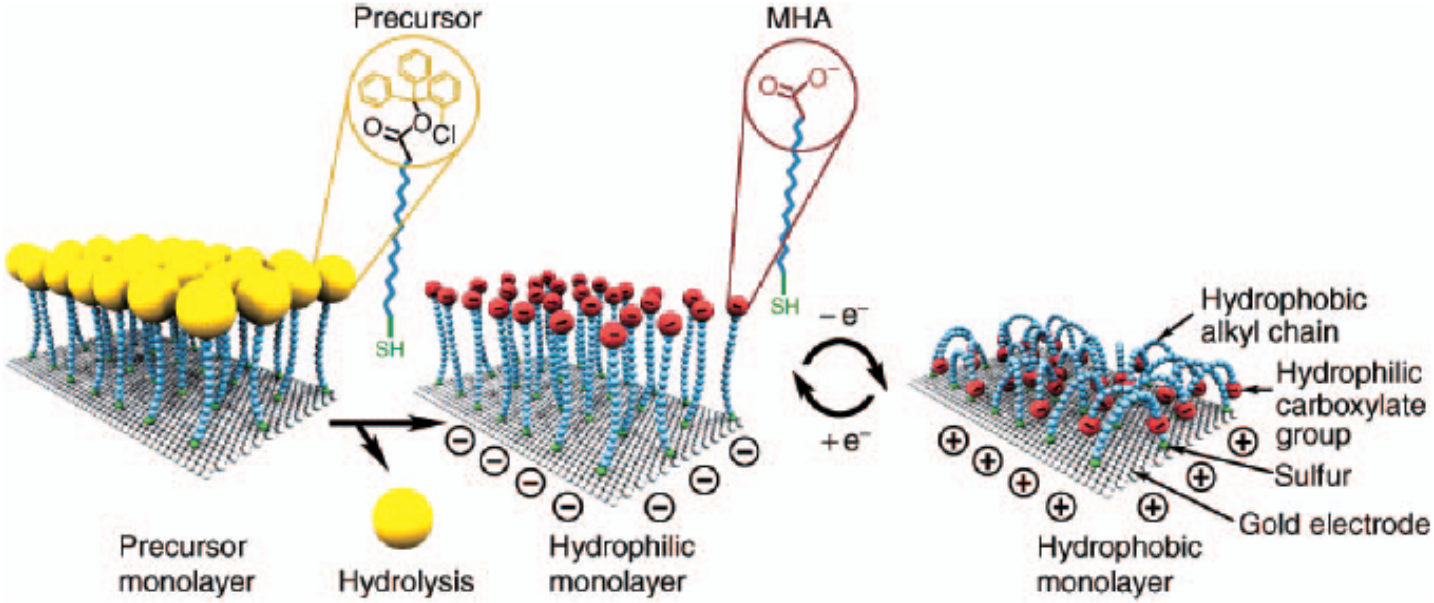

Figure 1. Idealized representation of the transition between straight (hydrophilic) and bent (hydrophobic) molecular conformations. Ions and solvent molecules are not shown. MHA is 16-mercapto-hexadecanoic acid. (Reproduced with permission from Reference 38.)

Temperature Responsive Surface

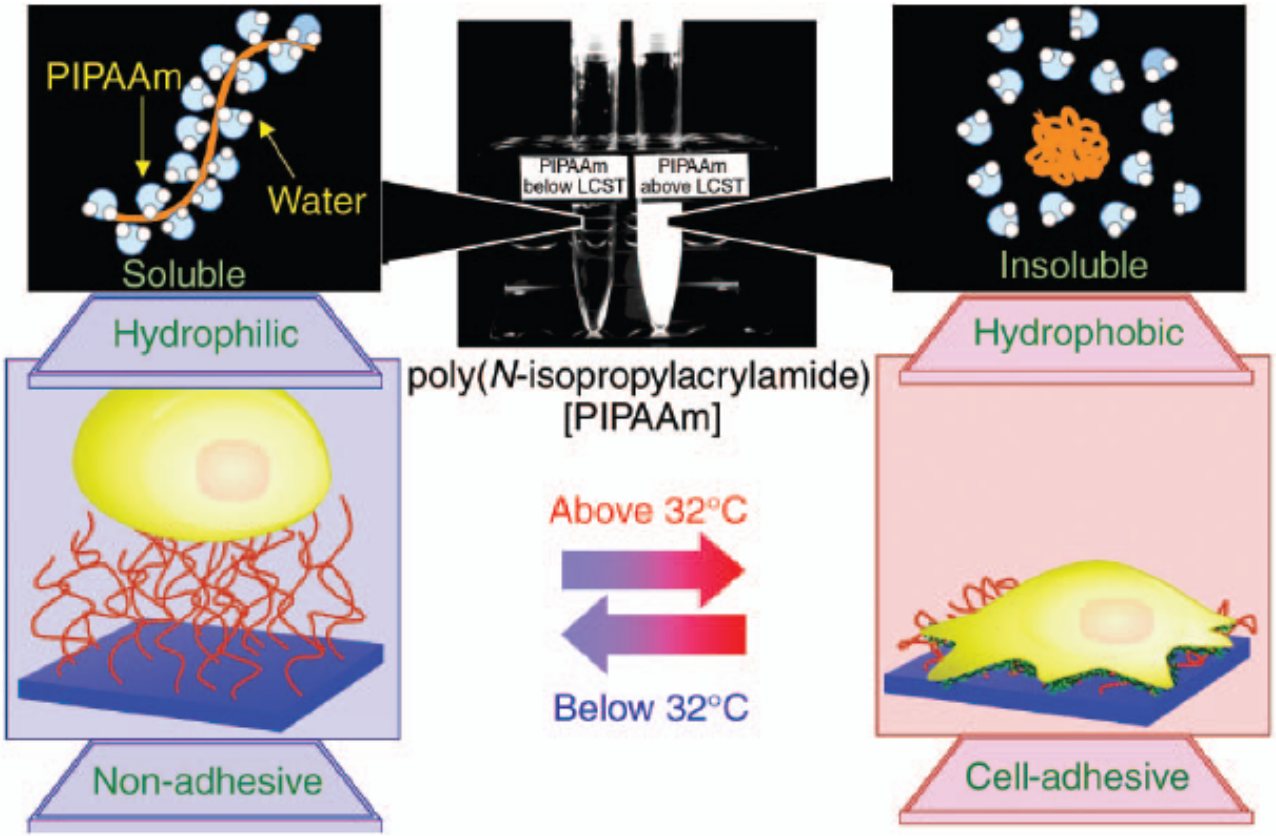

*Figure 1. Temperature-responsive culture dishes. The temperature-responsive polymer poly(*N*-isopropylacrylamide) (PIPAAm) exhibits a transition from hydrophobic to hydrophilic across its lower-critical solution temperature (LCST) of 32°C. After electron-beam polymerization and grafting to normal tissue-culture polystyrene (TCPS) dishes, temperature-responsive culture surfaces can be produced. The non-invasive harvest of various cell types as intact sheets, along with deposited extracellular matrix, can be achieved by reducing the culture temperature.*

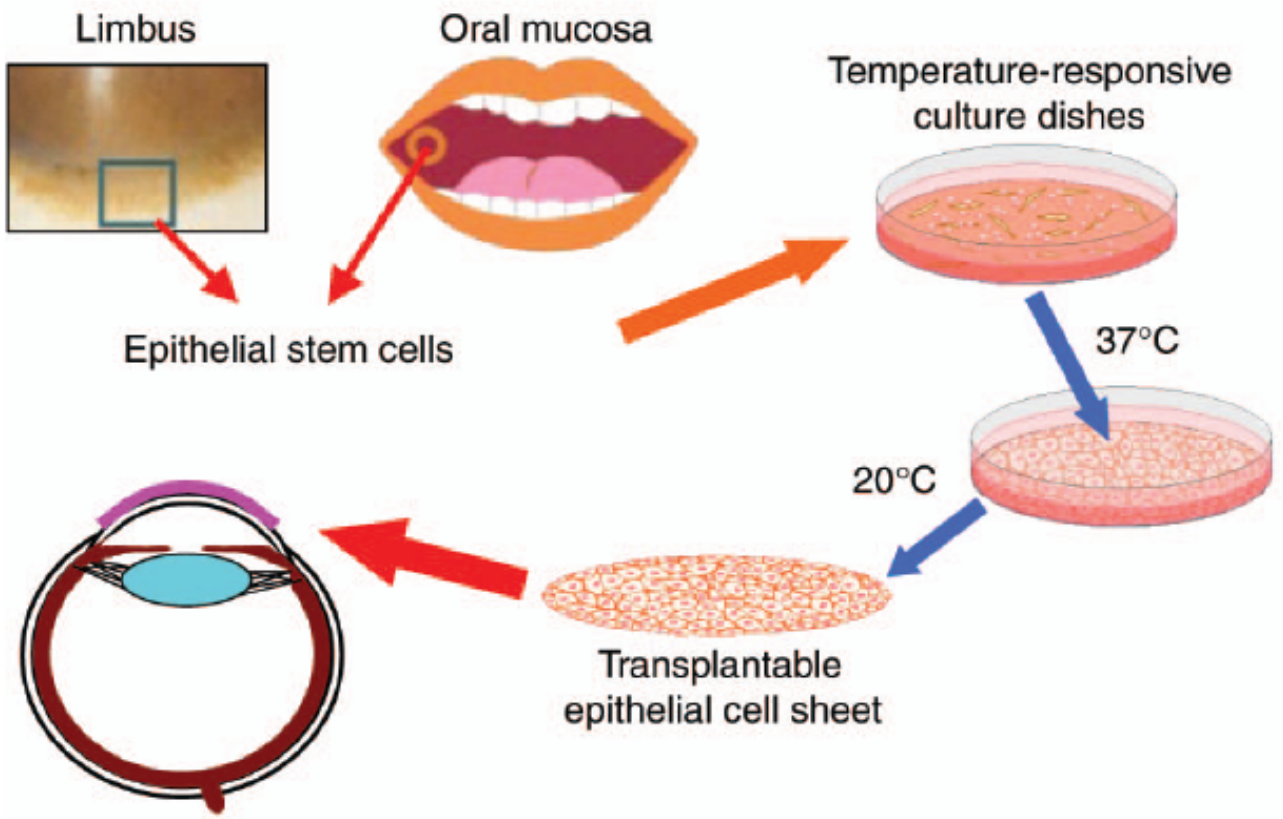

Figure 2. Corneal surface reconstruction. Small biopsies from the limbus (the border between the cornea and neighboring conjunctiva) or from oral mucosa provide for the isolation of epithelial stem cells. Cell sheets fabricated on temperature-responsive culture dishes can be harvested and transplanted directly to the ocular surface without the need for carrier substrates or sutures.

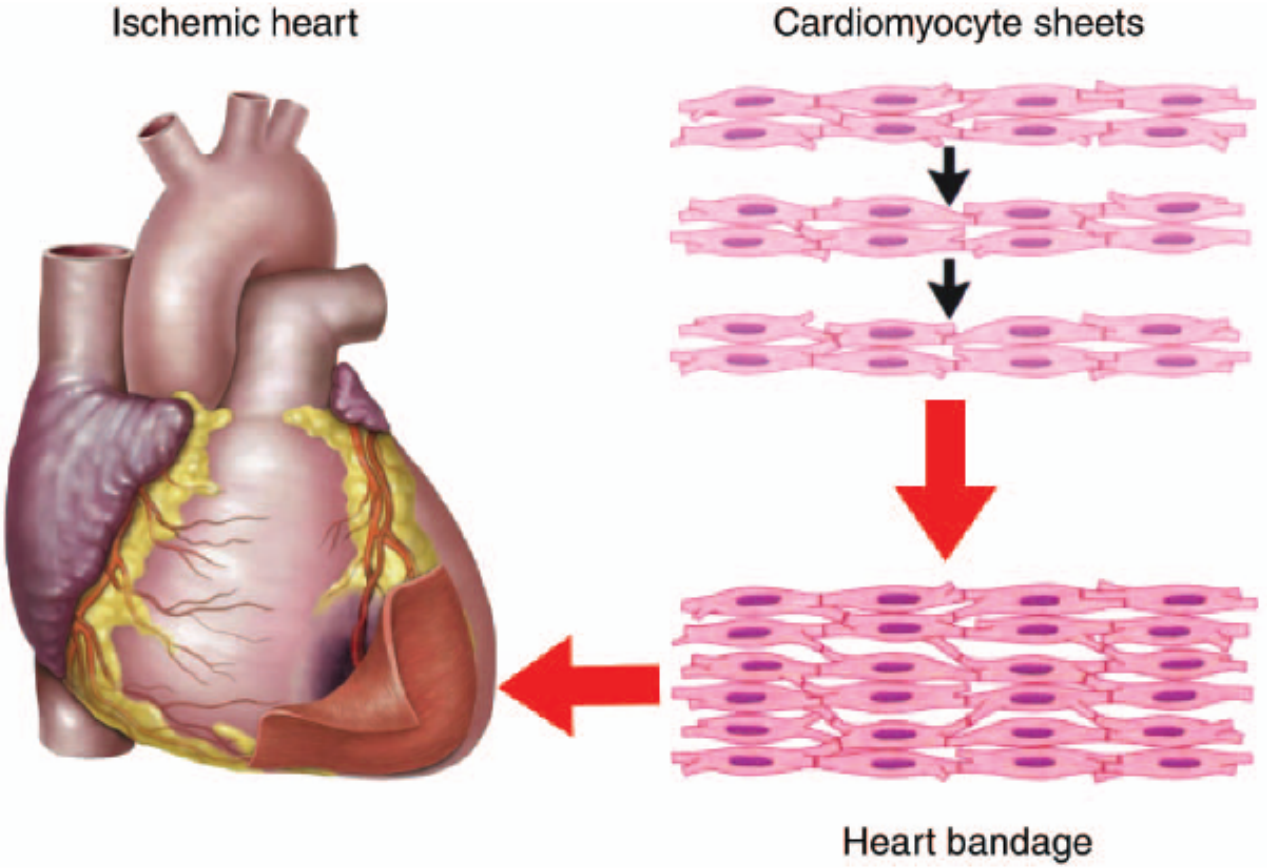

Figure 3. Myocardial cell-sheet engineering. Cardiomyocyte sheets harvested from temperature-responsive culture surfaces can be layered to form three-dimensional tissues that beat synchronously and simultaneously. We believe that layered cardiomyocyte sheets can act as a "heart bandage" for the recovery of ischemic cardiac tissue.

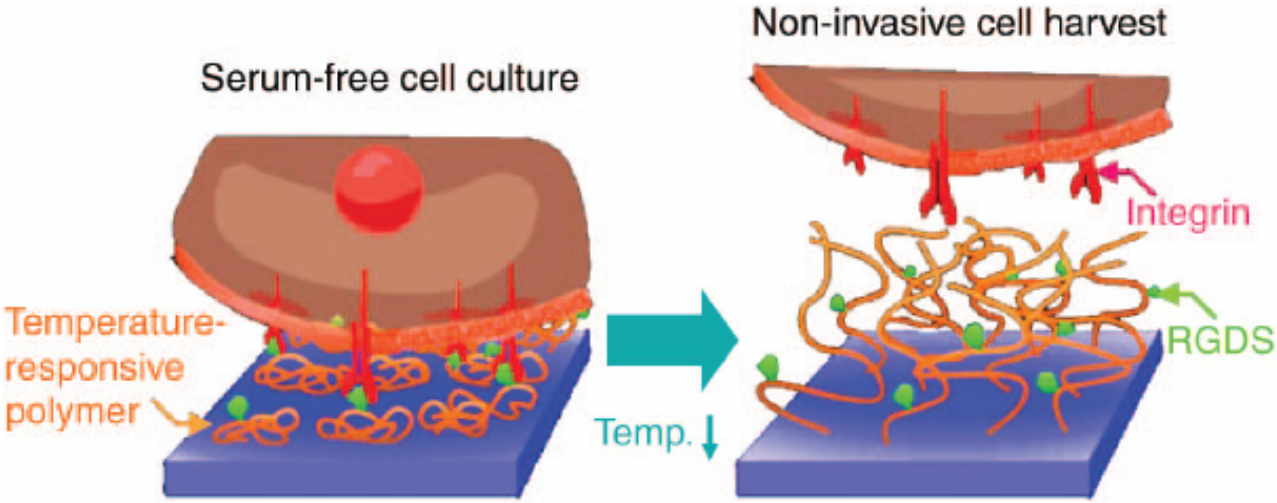

Figure 4. Immobilization of Arg-Gly-Asp-Ser (RGDS) peptides to temperature-responsive surfaces. Cells can be cultured in serum-free conditions by immobilizing the synthetic cell-adhesive RGDS peptide to temperature-responsive culture dishes. By decreasing the culture temperature, cells can still be non-invasively harvested, while the RGDS peptides remain attached to the temperature-responsive polymer surface.

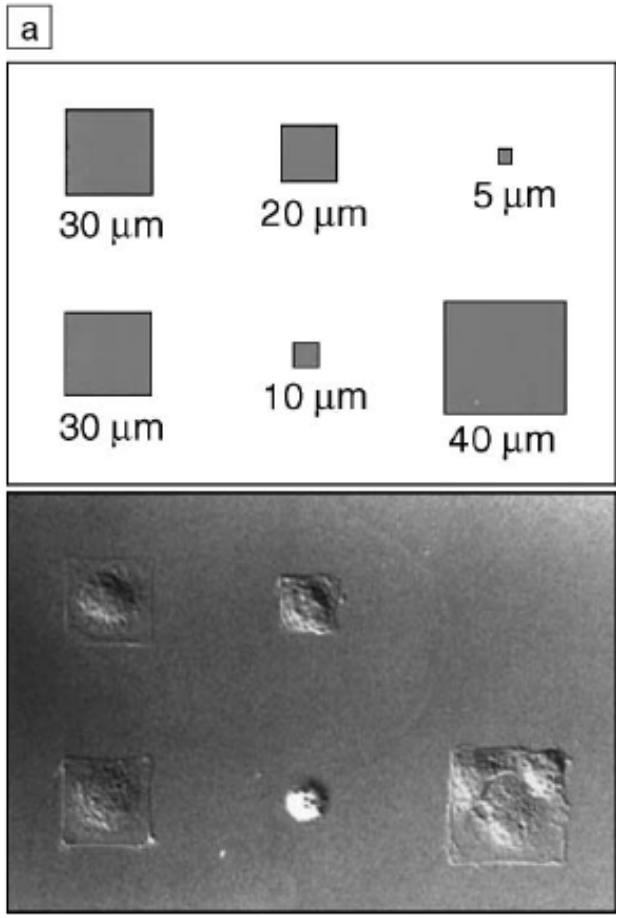

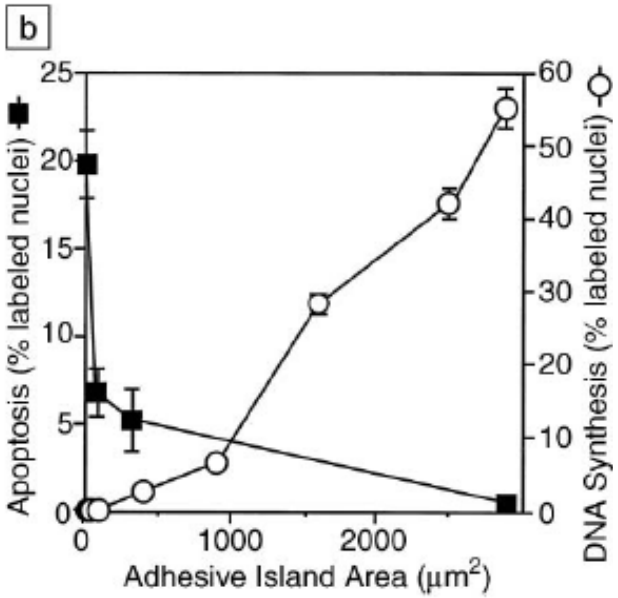

Figure 2. The influence of the footprint of a cell on its choice between growth and apoptosis. (a) (top) Schematic diagram showing the pattern: square islands of self-assembled monolayers (SAMs) to which proteins stick, surrounded by a different SAM to which proteins do not adsorb; (bottom) Nomarski microscopic image of the shapes of bovine adrenal capillary endothelial cells confined to the patterns. Scale labels indicate lengths of the sides of the squares. (b) Changes in cell shape as cells attach, spread, and flatten on an adhesive surface can regulate cell growth and death: apoptotic (cell death) index versus DNA synthesis (cell growth) index after 24 h, plotted as a function of the area of the spread cell.

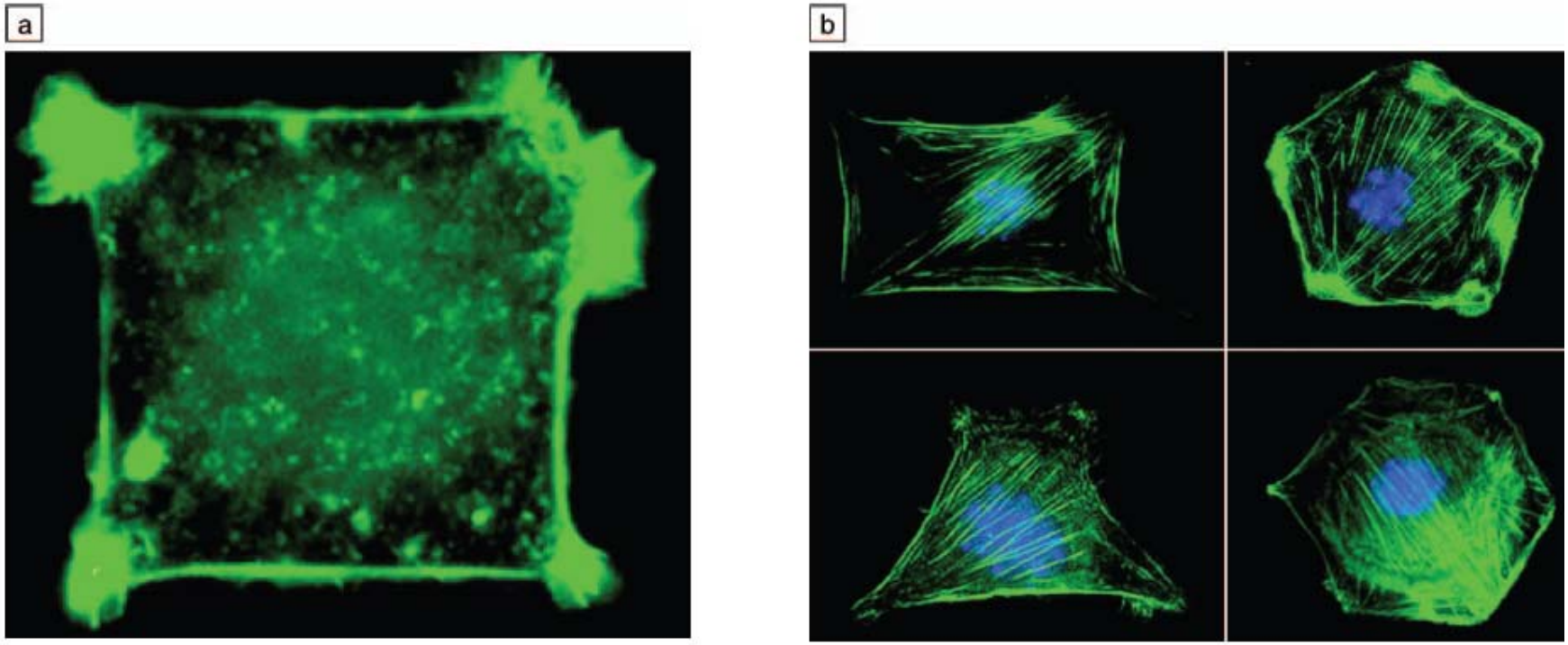

Figure 3. (a) A cell spread on a square 30 μm × 30 μm island; the cell was stimulated with platelet-derived growth factor (PDGF) and stained for F-actin with fluorophore-labeled phalloidin. (b) Cells confined to various shapes (all with areas of 900 μm^2) were stimulated with PDGF and stained with phalloidin and 4'-6-diamidino-2-phenylindole to visualize F-actin (green) and nuclei (blue). Images obtained by fluorescence microscopy.

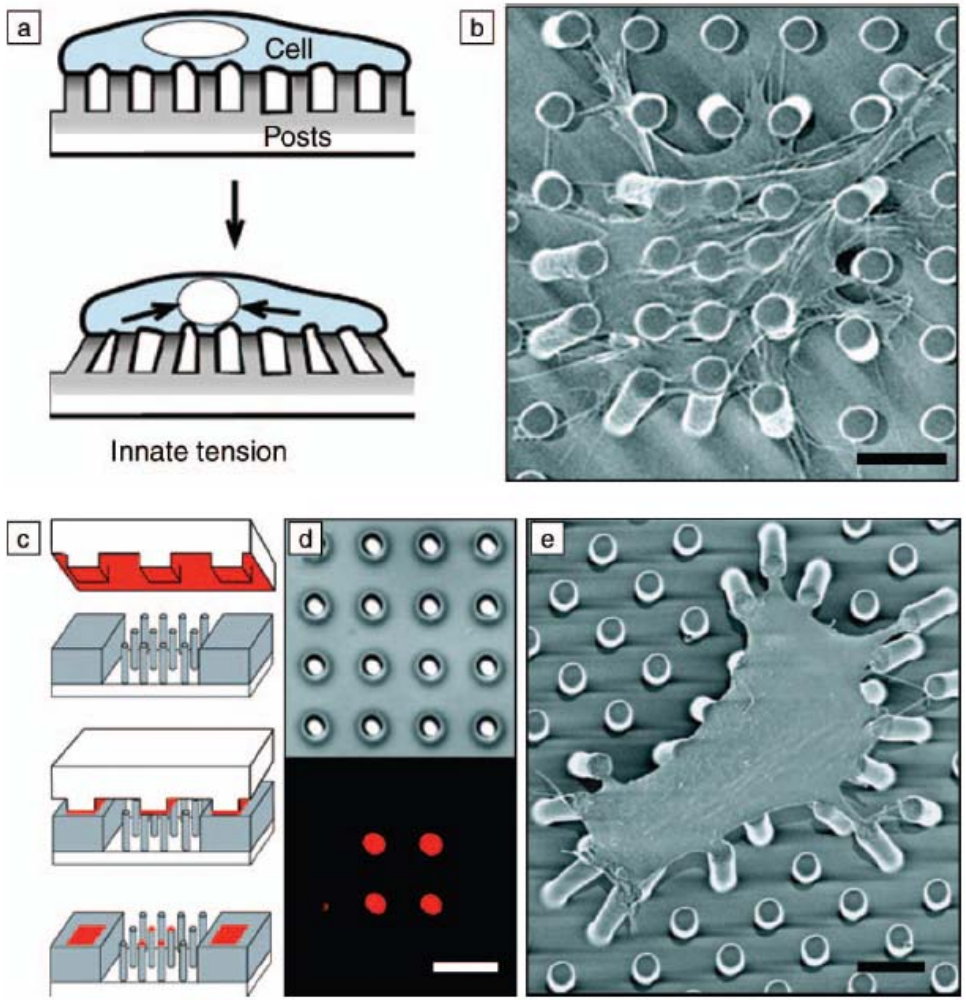

Figure 4. Elastomeric silicone microposts used to modulate the deformability of a substrate to cellular contractions. (a) Schematically, cells adhere to the tips of an array of closely spaced, vertically oriented elastomeric posts. When cells contact and probe the surface, the microposts deflect, depending on their mechanical stiffness, which can be easily manipulated by altering their dimensions. (b) Scanning electron micrograph showing a cell attached to the entire micropost substrate, including the shafts of the microposts and the underlying base. (c) Schematic illustration showing the process for microprinting adhesive proteins on the microposts. (d) Differential interference contrast (top) and immunofluorescence (bottom) micrographs of the same region of posts where a 2 × 2 array of posts has been printed with fibronectin. When adhesive proteins are selectively microprinted on the tips of the microposts (e), cells only attach on the tips. Scale bars indicate 10 μm.

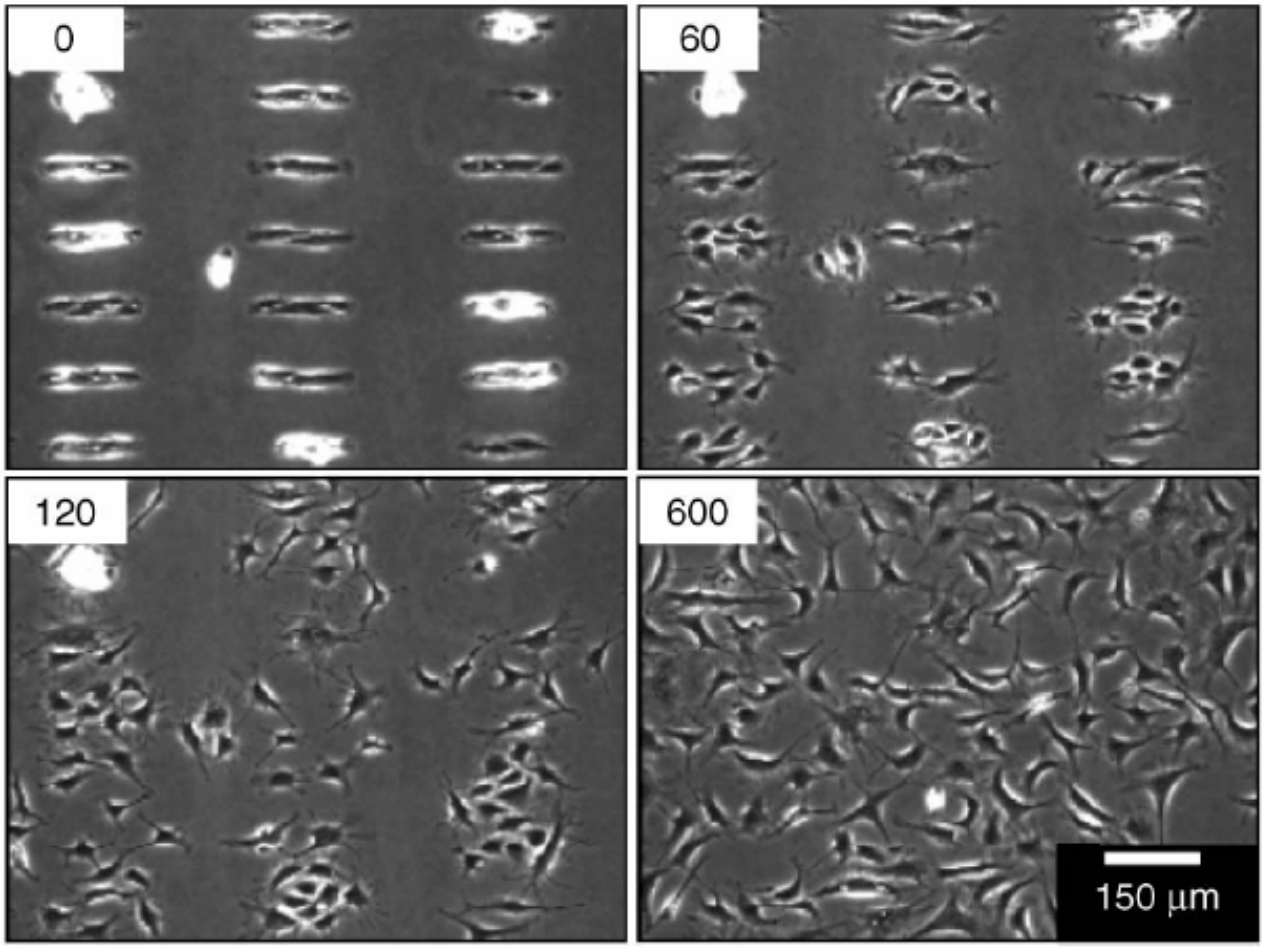

Figure 5. Bovine capillary endothelial cells were initially confined to rectangular patterns using methyl-terminated self-assembled monolayers (SAMs) surrounded by ethylene-glycol–terminated (EG-terminated) SAMs. Application of a cathodic voltage pulse (–1.2 V for 30 s) released the cells from the constraints of the microislands by desorbing the EG-terminated SAMs and enabling proteins to adsorb from the culture medium that allowed the attachment and movement of cells. The numbers indicate the time elapsed (in minutes) after the voltage pulse.

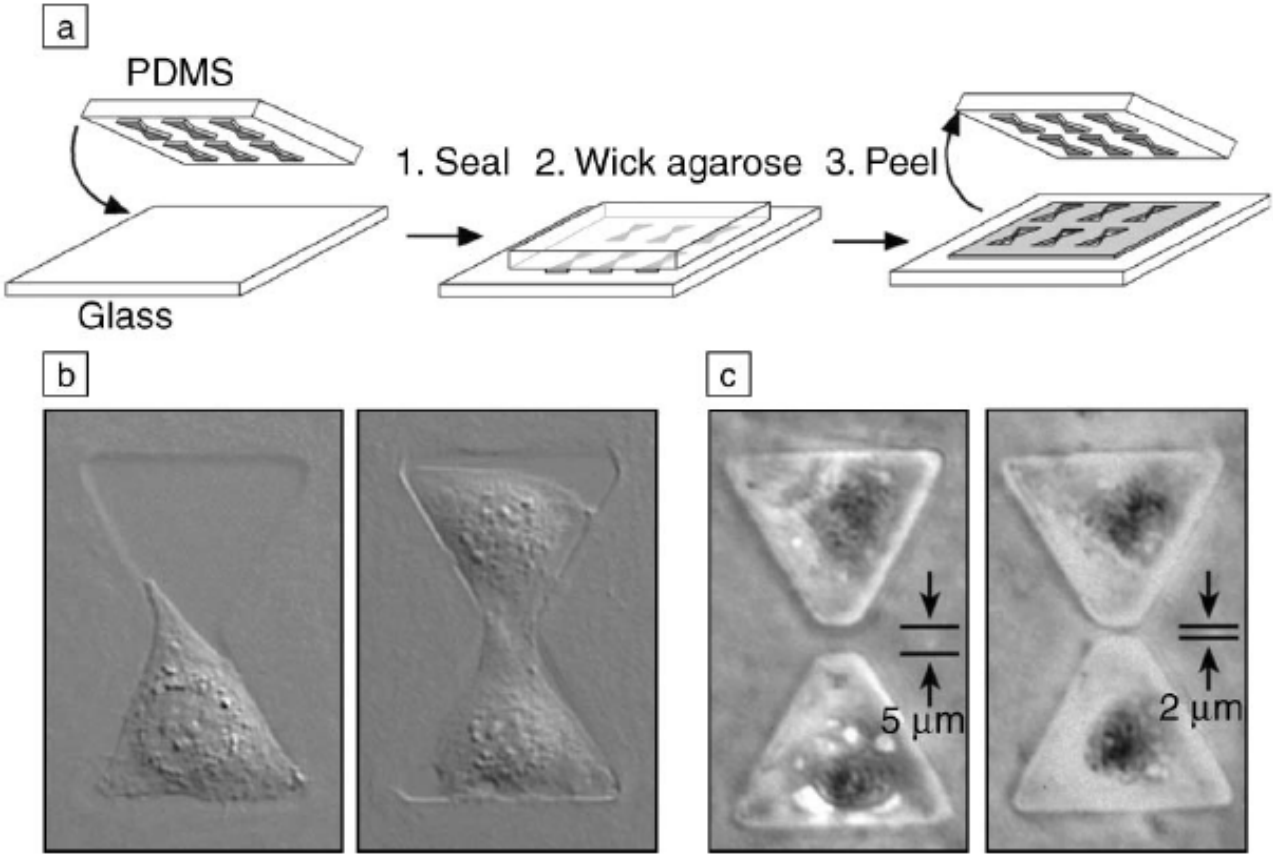

Figure 6. Method to induce cells to culture in pairs with control over the contact between them. (a) Agarose is wicked into channels formed by a poly(dimethylsiloxane) stamp sealed against a glass coverslip and allowed to gel before the stamp is peeled off. (b) When cells are seeded onto these substrates containing bowtie-shaped wells, cells attach and culture as either single cells or pairs. (c) The single cell-to-cell contact formed in these pairs can be blocked by fabricating substrates in which the agarose forms a thin wall, cutting the bowtie-shaped wells into separate, although closely spaced, wells.